Direct Hydrocarbon Solid Oxide Fuel Cells

Steven McIntosh and Raymond J. Gorte*

Department of Chemical and Biomolecular Engineering, University of Pennsylvania, Philadelphia, Pennsylvania 19104

Contents

1. Introduction

The promise of direct and efficient conversion of chemical to electrical energy makes fuel cell development an area of great technological interest. The advantages over traditional power generation systems are numerous. Most prominent is the increased efficiency associated with directly converting chemical energy to electrical energy. Fuel cells are not subject to the Carnot-cycle limitations, and unlike high-efficiency turbines, exhibit their highest efficiency at low loads. Fuel cells do not produce significant quantities of NO_x, SO_x, or particulate pollutants. Compared to normal batteries, fuel cells can have much higher energy densities and can be recharged more quickly and easily. Finally, fuel cells can be applied in applications that require both low and high power outputs, and they can be modular and portable.

One of the main limitations of current fuel cell technologies is the requirement that the fuel be

* Author to whom correspondence should be addressed. E-mail; gorte@seas.upenn.edu. Tel: (215) 898-4439. Fax: (215) 573-2093.

Steven McIntosh was born in Dundee, Scotland in 1977. He received his Batchelor of Engineering in Chemical Engineering from the University of Edinburgh in 1999. He is currently completing his Ph.D. degree at the University of Pennsylvania. The focus of his thesis is the development and characterization of direct-hydrocarbon solid oxide fuel cells. After a postdoctoral year, he will start as an Assistant Professor in Chemical Engineering at the University of Virginia in 2005.

Dr. R. J. Gorte joined the faculty at the University of Pennsylvania in 1981 after receiving his Ph.D. from the University of Minnesota. He is currently the Russell Pearce and Elizabeth Crimian Heuer Professor of Chemical Engineering. Since joining Penn, Dr. Gorte has served as Chairman of Chemical Engineering from 1995 to 2000 and was the Carl V. S. Patterson Professor of Chemical Engineering from 1996 through 2001. He has received a number of awards, including the 1997 Parravano Award of the Michigan Catalysis Society, the 1998 Philadelphia Catalysis Club Award, the 1999 Paul Emmett Award of the North American Catalysis Society, and the 2001 Penn Engineering Distinguished Research Award. He is on the Board of Editors of *Journal of Molecular Catalysis A* and the *Journal of Catalysis*.

hydrogen. Although hydrogen is often referred to as being the ideal fuel of the future, there are a number of problems relating to hydrogen generation and storage that must be overcome before it can be

implemented on a wide scale. One of the biggest problems is that, at the present time, an estimated 96% of hydrogen is produced by reforming hydrocarbons,[1] and even with highly optimized large-scale production, between 20 and 30% of the fuel value of the hydrocarbons is lost during this process.[1] A second major problem for portable applications is fuel storage since it is difficult and expensive to store hydrogen in a form that has an energy density comparable to that of hydrocarbon liquids. Until other sources of hydrogen become available and hydrogen-storage problems are resolved, it is difficult to see how hydrogen can make major inroads as a fuel supply.

A major advantage of solid oxide fuel cells (SOFC) is that they have much greater fuel flexibility due to the fact that O^{2-} anions are the species transported through the membrane. This allows SOFC to operate, in principle, on any combustible fuel. A second advantage of SOFC is that they operate at high temperatures where the waste heat can be used either for running steam turbines or for running the endothermic, steam-reforming reactions. Indeed, both of these concepts are used in prototype SOFC units. The high operating temperatures of SOFC, required for sufficient oxygen-ion conductivity, are an advantage for utilizing waste heat. While the high operating temperatures have caused early work on SOFC to be focused on large-scale applications, a number of groups are currently working on small to medium sized systems for battery replacement and auxiliary power units.[2-11]

There have already been a number of excellent reviews describing many aspects of SOFC,[12-23] and we will not try to duplicate that literature. For information on stack designs and cells operating on H_2 or on synthesis gas (a mixture or H_2 and CO) produced by reforming, we refer the reader to those other reviews. In this review, we will focus on recent work aimed at operating SOFC directly on hydrocarbon fuels and on anode materials that are compatible with direct hydrocarbon utilization. We have further restricted the scope to the performance and analysis of single-cell systems. While stacks that operate directly on hydrocarbons will likely need to be different from more traditional stacks, the development of direct-utilization SOFC is still in its infancy, with only one report of preliminary data on the stack level.[24]

We will begin this paper with a very brief tutorial covering the fundamental principles of SOFC operation before examining the important issues and current status of research relating to direct-utilization SOFC. The most critical issue for SOFC operating on hydrocarbon fuels without reforming is the need for anodes that do not catalyze carbon formation at the high SOFC operating temperatures. Because Ni-based anodes do not appear to be suitable for direct utilization, we will only briefly review work on these anodes. Finally, because relatively few groups have worked on direct utilization, this review will have a heavy emphasis on our own work at the University of Pennsylvania.

2. SOFC Fundamentals

2.1. Definition of Direct Utilization SOFC

There has been some controversy in the literature over precisely what should be called direct oxidation or direct utilization of hydrocarbons in an SOFC.[25] As pointed out by Marina and Mogensen[26] and Park et al.,[27] direct, electrochemical oxidation of complex hydrocarbons is unlikely to occur in one step. Even in the case of methane, the reaction produces eight electrons and must almost certainly occur in multiple steps.

It has been argued that all steps in the reaction must be electrochemical in nature for the process to be called direct oxidation.[25] According to this definition, any process that involves cracking of the hydrocarbon on the anode material, followed by electrochemical oxidation of the cracking products, should not be considered to be direct oxidation. The primary reason for using this narrow definition for direct oxidation is that the open-circuit voltage (OCV) of the cell will be equal to the theoretical, Nernst potential if there are no other losses and if all steps in the oxidation mechanism are electrochemical.

However, applying a similar definition to heterogeneous catalysts, one would probably conclude that there is no such thing as a hydrocarbon oxidation catalyst. For example, considering methane oxidation by O_2 over a heterogeneous Pd catalyst, the first step almost certainly involves C−H bond scission to form carbon-containing surface species on the Pd.[28] These surface species are then oxidized in subsequent steps. Using the same definition for heterogeneous oxidation as has been used for direct oxidation in SOFC, Pd should probably be considered a cracking catalyst that is also capable of oxidizing the cracking products. Similarly, it seems unlikely that electrochemical oxidation of hydrocarbons could ever occur without catalytic components in the anode promoting C−H and C−C bond scissions. Such a strict definition of direct oxidation based on mechanistic steps does not seem either practical or useful to us.

First, we will refer to the direct use of hydrocarbon fuels in an SOFC as direct utilization rather than direct oxidation. Second, we recognize that the broadest definition of direct utilization, exclusive from mechanistic considerations, should include rather conventional use of fuel by internal reforming, with steam being cofed to the fuel cell with the hydrocarbon. Indeed, this nomenclature has been used for many years with molten-carbonate fuel cells.[29,30] However, because internal reforming is essentially limited to methane and because the addition of steam with the fuel adds significant system complexity, we will focus primarily on systems and materials in which the hydrocarbons are fed to the fuel cell directly without significant amounts of water or oxygen.

2.2. Basic Operating Principles of SOFC

The operating principles behind an SOFC are shown schematically in Figure 1. Like all fuel cells, the SOFC consists of three main components: a
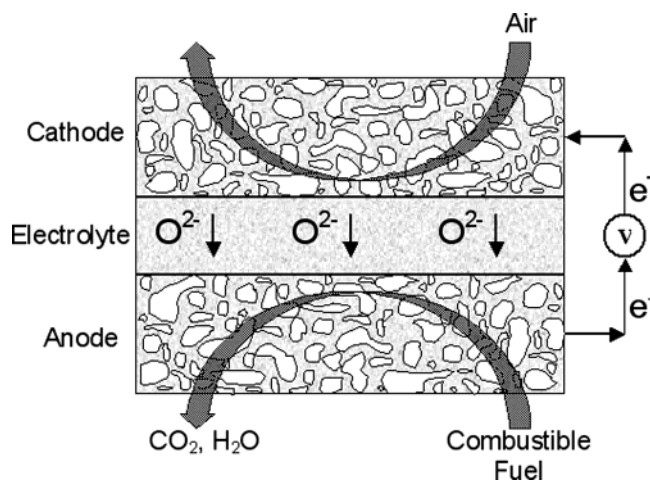
Figure 1. Schematic of SOFC operating principle. (Reproduced with permission from ref 171. Copyright 2003 Elsevier.)

cathode (or air electrode), an anode (or fuel electrode), and an electrolyte. The distinguishing feature of an SOFC is that the electrolyte is an ion-conducting ceramic and an electronic insulator. While proton-conducting ceramics are known,[31−36] the vast majority of work on SOFC has been performed with ceramics that are oxygen−anion conductors.

Under operation, molecular oxygen is reduced to oxygen anions using electrons supplied from an external circuit at the cathode, according to the following reaction:

$$O_2(g) + 4e^- \rightarrow 2O^{2-} \quad (1)$$
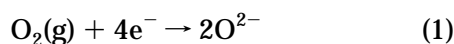
In addition to being able to catalyze the dissociation of O_2, the material used for the cathode must be electronically conductive in the presence of air at high temperature, a property found primarily in noble metals and electronically conductive oxides. Ionic conductivity is also desirable for extending the reaction zone well into the electrode since the ions must ultimately be transferred to the electrolyte. Since precious metals are prohibitively expensive when used in quantities sufficient for providing electronic conductivity, essentially all SOFC prototypes use perovskite-based cathodes, with the most common material being a Sr-doped $LaMnO_3$ (LSM).[15] In most cases, the cathode is a composite of the electronically conductive ceramic and an ionically conductive oxide, often the same material used in the electrolyte.

The electrolyte is probably the most crucial component of SOFC. It must be dense to separate the fuel and air compartments of the cell, and retain its high ion conductivity and low electronic conductivity over a very wide range of oxygen fugacities (referred to here as oxygen pressures, $P(O_2)$), from values close to 1 atm on the cathode side to values that could be below 10^{-20} atm at the anode. The operating temperature of the SOFC is set by the requirement for high ionic conductivity in the electrolyte and must be greater than approximately 973 K with yttria-stabilized zirconia (YSZ), the current material of choice.[15] While other materials having higher ionic conductivities at lower temperatures are being considered, most of these materials do not have the same

high stability and low electronic conductivity at low $P(O_2)$. Since decreased operating temperatures simplify the materials requirements in other parts of the SOFC, there is a trend toward using very thin electrolytes supported on one of the electrodes.

Driven by the difference in oxygen chemical potential between fuel and air compartments of the cell, oxygen anions migrate through the electrolyte to the anode where they are consumed by oxidation of the fuel according to eq 2.

$$C_nH_{2n+2} + (3n+1)O^{2-} \rightarrow$$
$$nCO_2 + (n+1)H_2O + (6n+2)e^- \quad (2)$$
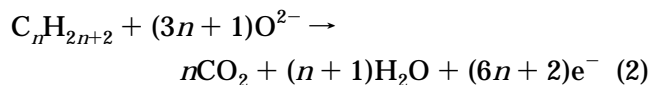
The electrons released by this reaction flow through an external circuit to the cathode to complete the circuit. Analogous to the cathode, the anode must be catalytically active for the oxidation reaction and retain sufficient electronic and ionic conductivities. For example, with the current state-of-the-art anode materials, which are Ni−YSZ, ceramic−metallic (cermet) composites, Ni provides the catalytic activity and electronic conductivity, while the YSZ component provides ionic conductivity and a thermal expansion match with the YSZ electrolyte. While metals other than Ni can be used in the anode, Ni is almost universally used because it is inexpensive, has excellent mechanical and electrical properties, and is a good steam-reforming catalyst. Typical cermets contain at least 30 vol % Ni to ensure high electronic conductivity through a fully percolated matrix.[37] However, a major limitation to Ni-based anodes is that Ni catalyzes the formation of graphitic carbon at low H_2O/C ratios, as we will discuss in more detail later in this review. Alternative materials have been suggested, including electronically conductive perovskites and Cu-based cermets.

Any one of the three components in SOFC, the cathode, anode, or electrolyte, can provide the structural support for the cells. Traditionally, the electrolyte has been used as the support; however, this approach requires the use of thick electrolytes, which in turn requires high operating temperatures. Electrode-supported cells allow the use of thin electrolytes. The Siemens−Westinghouse Corporation has developed a cathode-supported design,[38−40] although this has required electrochemical vapor deposition of the YSZ electrolyte. Most other groups have focused on anode-supported cells. In all cases, it is important to maintain chemical compatibility of those parts that come in contact and to match the thermal expansion coefficients of the various components. A large amount of research has been devoted to these important issues, and we refer the interested reader to other reviews.[15,16,18,19,41]

2.3. Anode Three-Phase Boundary

Because the performance of an SOFC depends strongly on the anode structure, it is useful to consider how the anode works on a microscopic scale.[42,43] The electrochemical reaction can only occur at the three-phase boundary (TPB), which is defined as the line at which the electrolyte, the electron-
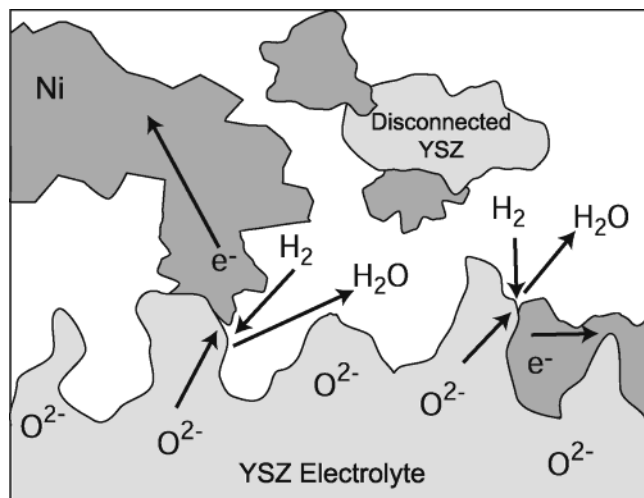
Figure 2. Schematic of Ni/YSZ anode three-phase boundary.

Table 1. Standard Cell Potential, $E°$, for Various Fuels at 973 and 1073 K (Reprinted with permission from ref 164. Copyright 2004 The Electrochemical Society, Inc.)

fuel	$E°$, 973 K (V)	$E°$, 1073 K (V)
hydrogen	1.01	0.98
carbon monoxide	0.99	0.98
methane	1.05	1.04
n-butane	1.13	1.12
toluene	1.13	1.12
n-decane	1.14	1.13

conducting metal phase, and the gas phase all come together. A cartoon of the region between the electrolyte and the anode where the TPB exists is shown in Figure 2. If there is a breakdown in connectivity in any one of the three phases, the reaction cannot occur. If ions from the electrolyte cannot reach the reaction site, if gas-phase fuel molecules cannot reach the site, or if electrons cannot be removed from the site, then that site cannot contribute to the performance of the cell. While the structure and composition clearly affect the size of the TPB, various theoretical and experimental methods have been used to estimate that, under normal conditions, the region in which the TPB exists extends no more than approximately 10 μm from the electrolyte into the electrode.[42,44–49] Essentially, so long as the diffusion of ions through the electrolyte partially limits the performance, the concentration of excess ions in the oxide phase of the anode will be insignificant beyond this distance.

The TPB concept has important implications for optimization of both anodes and cathodes. To facilitate transfer of O^{2-} to or from the electrolyte, it is necessary to have fingers of the electrolyte material extending from the electrolyte, into the electrode. A detailed analysis of the role of these fingers has been carried out for cathodes,[48,50–52] and similar concepts are almost certainly applicable to the anode. It is important to note that the electrolyte material within the electrode is only effective if it is sintered to the electrolyte itself. When oxide particles are simply pressed together at low temperatures, there will be large grain-boundary resistances that will prevent the free flow of oxygen anions. Removing the grain-boundary resistance between YSZ particles typically requires a sintering temperature of at least 1500 K.

While high temperatures do not severely limit fabrication of Ni–YSZ cermets, they can impact the way in which other composite electrodes are made. This is well-known for cathodes, where the most commonly used material is a composite of YSZ and Sr-doped $LaMnO_3$ (LSM). The primary reason for using LSM, rather than materials such as Sr-doped $LaFeO_3$ (LSF) or $LaCoO_3$ (LSC) that exhibit a better performance, is that LSM–YSZ mixtures can be

heated to higher temperatures before undergoing a solid-state reaction with YSZ.[41,53–55] When Ni is replaced by other metals or by electronically conductive ceramics, the issue of reaction with YSZ at the anode sintering temperatures must be revisited.

2.4. SOFC Thermodynamics

The maximum electrical energy available from a fuel cell is determined by the Gibbs free energy difference across the electrolyte membrane, ΔG. This determines the equilibrium voltage of the cell, E, through the Nernst equation, which is nothing more than a restatement in electrical units of how ΔG (= $2FE$) changes with pressure.

$$E = (RT/2F) \ln\{P(O_{2\,cathode})^{1/2}/P(O_{2\,anode})^{1/2}\} \quad (3)$$

In this equation, F is Faraday's constant, the product of Avogadro's constant and the charge on an electron. Since fuel, not a mixture of O_2, is fed to the anode, $P(O_{2\,anode})$ is assumed to be fixed by the equilibrium relationship. For example, with H_2 as the fuel

$$P(O_{2\,anode})^{1/2} = \\ \exp\{-\Delta G°/RT\}P(H_2O_{anode})/P(H_{2\,anode}) \quad (4)$$

and eq 3 becomes

$$E = E° + (RT/2F) \ln\{P(H_{2\,anode})P(O_{2\,cathode})^{1/2}/ \\ P(H_2O_{anode})\} \quad (5)$$

Here, we have substituted $E°$, the standard potential for oxidation of H_2, for $-2F\Delta G°$, where $\Delta G°$ is the free energy change for reaction under standard conditions. Obviously, similar relationships can be written to calculate the equilibrium potentials for other fuels. For example, for alkanes, C_nH_{2n+2}, the analogous relationship between partial pressures and the equilibrium cell potential is the following

$$E = E° + (RT/2(3n+1)F) \times \\ \ln\{P(C_nH_{2n+2\,anode})P(O_{2\,cathode})^{(3n+1)/2}/ \\ P(H_2O_{anode})^{n+1}P(CO_{2\,anode})^n\} \quad (6)$$

At the temperatures of interest for SOFC applications, the standard potentials for oxidation, E_o, are similar for hydrocarbon fuels and for H_2 and CO, as shown in Table 1. Since E_o for H_2 is more temperature dependent than the E_o for hydrocarbons, the thermodynamic advantage for hydrocarbon fuels is more apparent at higher temperatures. However, the
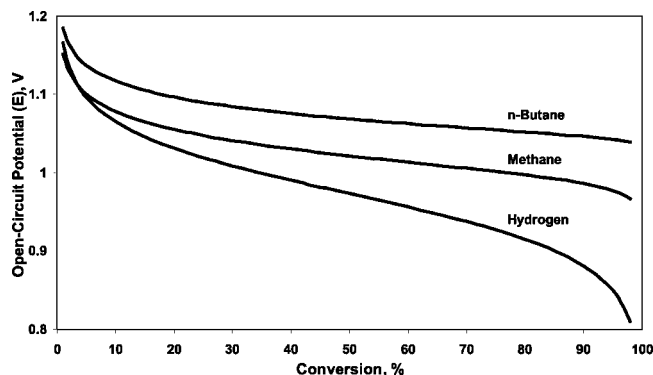
Figure 3. Theoretical open-circuit potential as a function of conversion to total oxidation of hydrogen, methane, and n-butane at 973 K.

standard potentials tell only part of the story since the theoretical Nernst potentials for hydrocarbons are not as dependent on fuel conversion. This is shown in Figure 3, where the Nernst potentials for H_2, CH_4, and n-butane, calculated from eqs 5 and 6, are shown as a function of conversion at 973 K. For these calculations, the hydrocarbons were assumed to react directly to CO_2 and H_2O, with no intermediate products, so that $P(H_2O_{anode})$ and $P(CO_{2\ anode})$ were determined from the stoichiometry of the reaction. The effect of conversion on the equilibrium potential is quite pronounced for H_2 in that the potential drops by 15% between 10 and 80% conversion. However, for the hydrocarbon fuels, the effect of conversion is much less, with a decline of only 1% over the same range for n-butane. Essentially, the hydrocarbons act as a buffer to prevent changes in $P(O_2)$; this buffering of $P(O_2)$ increases with the size of the hydrocarbon. The implication of this result is that the thermodynamic efficiency of a fuel cell operating directly on hydrocarbon fuels can be significantly higher.

2.5. SOFC Electrode Losses

In an ideal fuel cell, the efficiency is $\Delta G/\Delta H$.[56] Since this ratio can be close to unity, the losses could be negligible. In practice, the energy losses in the fuel cell are significantly higher. To calculate the electrical energy derived from a given amount of fuel using a fuel cell, one can simply take the product of the number of electrons produced times the potential of those electrons. Therefore, for a fixed amount of fuel, energy losses occur if either the number of electrons that are produced decreases or if the cell potential decreases.

The number of electrons produced per molecule is an important issue for hydrocarbons. While the addition of H_2O to the fuel for steam reforming has no effect on electron production, reforming of hydrocarbons larger than methane is usually accomplished through partial oxidation, with the ideal reaction shown in eq 7

$$C_nH_{2n+2} + (n/2)O_2 \leftrightharpoons nCO + (n+1)H_2 \quad (7)$$
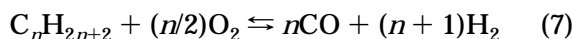
Whereas a mole of C_nH_{2n+2} is capable of producing $6n + 2$ electrons, the ideal products from the partial oxidation can produce only $4n + 2$ electrons. If the electrons are produced with the same potential in

both cases, the partial oxidation of the alkanes results in the loss of approximately 30% of the total energy available in the fuel. In other words, while the conventional calculation of the efficiency of the reforming process is based on the enthalpy difference between the initial hydrocarbon fuel and the CO and H_2 produced from that fuel, the efficiency is more properly calculated from the change in the Gibbs free energies of the alkane reactant and the CO and H_2 products. The free energies are reflected in the standard potentials, and since the standard potentials at the normal SOFC operating temperatures are essentially the same for hydrocarbon fuels as for H_2 and CO (see Table 1), the electron counting we have performed here accurately reflects the true loss in the energy of the fuel.

The cell potential is simply the work that can be accomplished by the electrons produced in the SOFC, and this potential decreases from the equilibrium value due to losses in the electrodes and the electrolyte. For YSZ electrolytes, the losses are purely ohmic and are equal to the product of the current and the electrolyte resistance. Within the electrodes, the losses are more complex. While there can be an ohmic component, most of the losses are associated with diffusion (both of gas-phase molecules to the TPB and of ions within the electrode) and slow surface kinetics. For example, concentration gradients for either O_2 (in the cathode) or H_2 (in the anode) can change the concentrations at the electrolyte interface,[57-59] which in turn establish the cell potential. Similarly, slow surface kinetics could result in the surface at the electrolyte interface not being in equilibrium with the gas phase.

An interesting point in this regard is that the complexity of hydrocarbon oxidation reactions allows for the possibility that equilibrium may be established with partial oxidation reactions, which may or may not be observable in the gas phase. For example, for cells with Cu/CeO$_2$/YSZ anodes, we have found the measured OCV in humidified methane to be ~250 mV lower than that predicted by equilibrium with total oxidation products, even though the same cell gave good agreement between measured and predicted OCVs in H_2.[60] Furthermore, in that same study, the addition to the anode of a precious metal catalyst increased the measured OCV for methane and had no effect on the OCV for H_2. This observation could be explained by an equilibrium between methane and partial oxidation products, such as formaldehyde; however, measurements of the gas-phase products showed that the total oxidation products, CO_2 and water, were produced in amounts consistent with methane consumption.[61] Therefore, the lower OCV with methane is likely due to the establishment of partial oxidation products that remain on the surface of the anode, or nonelectrochemical surface reactions, as discussed in Section 1.2. These losses are not observed with oxidation of H_2 because only one stable product, water, can be formed with this fuel. In the case of methane, it is noteworthy that the addition of precious metal catalysts to the anode could significantly increase the measured OCV.[60]

2.6. Electrode Characterization

A more complete discussion of characterization techniques is given elsewhere;[14] however, we wish to make a few important points here before discussing specific electrode materials. Prior to discussing techniques, it is important to recognize that electrode characterization is difficult and that there are large discrepancies in the values that have been reported in the literature for common electrode materials. For example, a brief survey of the recent literature on LSM−YSZ composite electrodes indicates a cathode ASR (area specific resistance; the losses can be calculated by multiplying this value with the current density) between 27[62] and 2.49[63] ohm cm² for cathodes operating at 973 K in air. On the other hand, Kim et al.[58] reported a total cell ASR of 0.28 ohm cm² at 0.7 V using a cell with an LSM−YSZ cathode. While part of the variability in reported ASR for LSM−YSZ cathodes is due to differences in the materials used in the various studies, at least some of the differences appear to be due to issues surrounding the measurement of electrode losses.[64] We suggest that the inherent difficulties associated with measuring LSM−YSZ losses will also manifest themselves in the characterization of other cathode and anode materials.

The two main techniques for measuring electrode losses are current interrupt and impedance spectroscopy. When applied between cathode and anode, these techniques allow one to separate the electrode losses from the electrolyte losses due to the fact that most of the electrode losses are time dependent, while the electrolyte loss is purely ohmic. The instantaneous change in cell potential when the load is removed, measured using current interrupt, can therefore be associated with the electrolyte. Alternatively, the electrolyte resistance is essentially equal to the impedance at high frequency, measured in impedance spectroscopy. Because current-interrupt is simply the pulse analogue to impedance spectroscopy,[14] the two techniques, in theory, provide exactly the same information. However, because it is difficult to make a perfect step change in the load, we have found impedance spectroscopy much easier to use and interpret.

To illustrate the use of impedance spectroscopy in analyzing cell performance, we consider data obtained on a cell with a Cu−ceria−YSZ anode, operating in H_2 and n-butane at 983 K. Figure 4 shows the V−I curves for H_2 and n-butane on an electrolyte-supported cell with a 550 μm electrolyte.[65] For H_2, the curve is essentially linear for current densities ranging from 0 to 400 mA/cm², while the V−I curve for n-butane is highly nonlinear over this range of current densities. The impedance spectra for H_2 and n-butane, taken as a function of current density, are shown in Figure 5. For H_2, the spectra are essentially independent of current density. The ohmic resistance that we associate primarily with the electrolyte, R_Ω, is obtained from the high-frequency intercept of the Cole−Cole plot with the real axis, 2.5 Ω cm², while the total cell impedance, 4.0 Ω cm², is obtained from either the low-frequency intercept in the Cole−Cole plot or from the slope of the V−I curve. The total
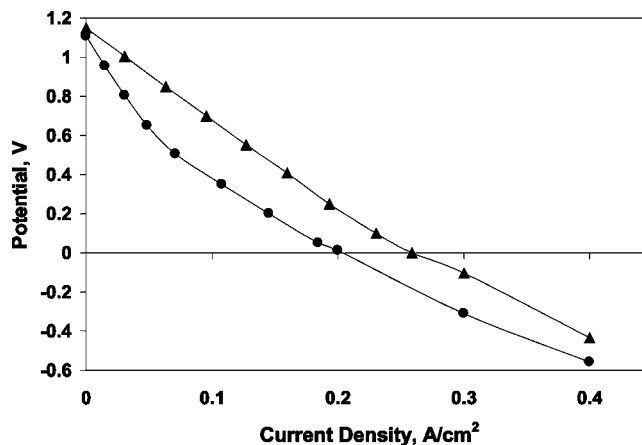
Figure 4. Cell potential as a function of current density for a 550-μm electrolyte-supported cell at 973 K in H_2 (▲) and n-butane (●) fuels. (Reprinted with permission from ref 65. Copyright 2003 The Electrochemical Society, Inc.)
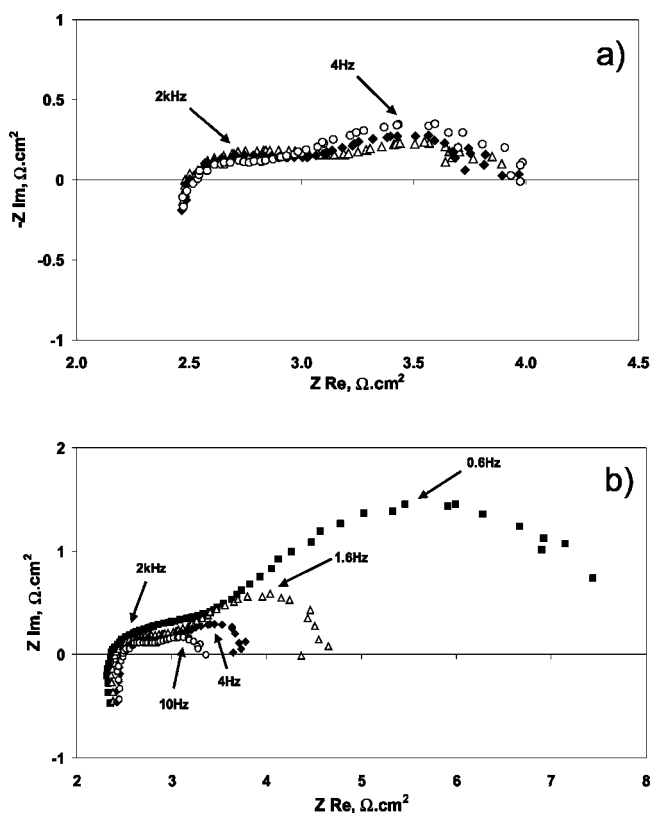
Figure 5. Two-probe impedance spectra measured at (■) 50, (△) 100, (◆) 200, and (○) 400 mA/cm² for (a) H_2 and (b) n-butane fuel at 973 K. (Reprinted with permission from ref 65. Copyright 2003 The Electrochemical Society, Inc.)

electrode impedance, R_E, is the difference between the total cell impedance and R_Ω. For n-butane, the curvature in the V−I curve is manifested in the fact that R_E changes with current density, as shown in Figure 5b. Since the cathode and electrolyte were the same for H_2 and n-butane, the differences between the two sets of data must be associated with additional anode losses with n-butane as fuel.

In general, it is necessary to have a reference electrode to separate anode and cathode losses. In this case, the impedance spectrum between reference and either anode or cathode allows one to determine the electrode loss from the nonohmic part of the
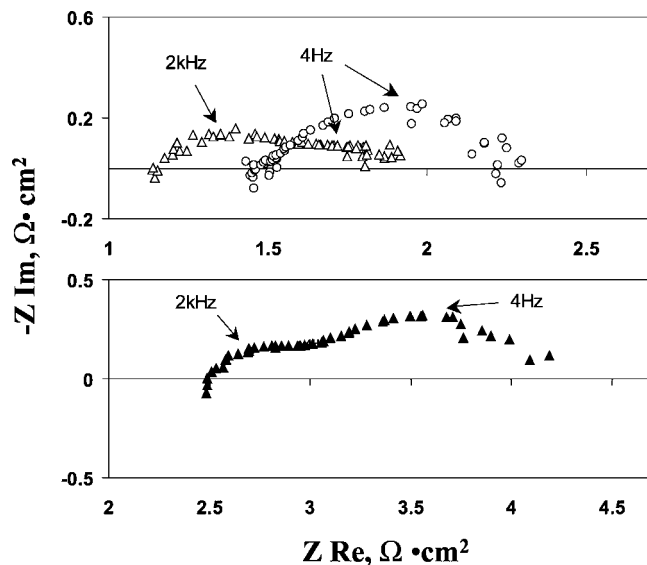
Figure 6. Impedance spectra for a 550-μm electrolyte-supported cell at 983 K and 350 mA/cm^2 using H$_2$. Ref $\rightarrow$ cathode ($\triangle$) and ref $\rightarrow$ anode ($\bigcirc$) and anode $\rightarrow$ cathode ($\blacktriangle$). (Reprinted with permission from ref 65. Copyright 2003 The Electrochemical Society, Inc.)

spectrum. This is illustrated in Figure 6, where the reference-to-cathode and reference-to-anode spectra are shown for the same cell as that discussed in the previous paragraph, using H$_2$ as the fuel. It is noteworthy that the ohmic resistances in both spectra are almost the same, and almost exactly one-half of the total ohmic resistance of the cell, showing that the reference electrode is sampling the potential at the center of the electrolyte. Furthermore, the characteristic frequencies for the anode and cathode spectra, 4 and 2 kHz, are also different. For this cell, the anode and cathode impedances are 1.1 and 0.4 Ω cm^2, respectively.

However, it should be recognized that improper placement of the reference and working electrodes will give erroneous results,[65-71] and even a small overlap of the working electrodes can lead to serious errors. For example, it is common practice to attach a reference electrode on the electrolyte, next to the cathode, on anode-supported cells. For this configuration, it is easily shown that all of the anode losses appear as cathode losses.[65] This error may, in some cases, lead to the belief that anode losses are negligible as compared to cathode losses, when the opposite may in fact be true. Furthermore, even with perfect alignment of the working electrodes, differences in the characteristic frequencies of the two electrodes can lead to losses in one of the electrodes appearing in the other electrode.[65,69] Indeed, it is for this reason that we avoid current-interrupt methods since they do not allow one to determine the characteristic frequencies associated with the electrode losses and therefore to observe this type of measurement error.

3. Carbon Formation

A primary issue in the operation of any fuel cell using hydrocarbon fuels, whether or not steam is present with the hydrocarbon fuel, is the requirement
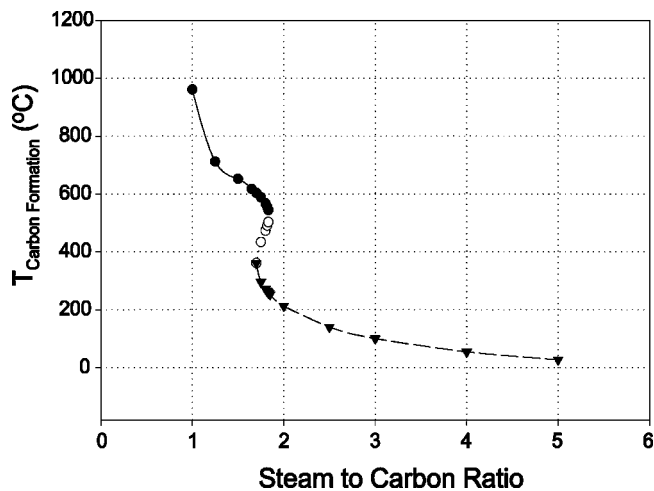
Figure 7. Carbon formation temperature for n-octane fuel as a function of steam-to-carbon ratio.[76]

that the fuel cell not be fouled by deposition of carbon-containing residues. At the high operating temperatures of an SOFC, hydrocarbons can react on the surfaces of the anode, on the interconnect plates, and on the tubing leading into the anode. Hydrocarbons can also react in the gas phase via free-radical cracking and polymerization, forming tars that can then deposit on the anode surfaces. Because of this issue, it is common to map the region of stability for hydrocarbon fuels based on thermodynamic calculations of carbon stability.[72-75] For example, Figure 7 shows a stability diagram for steam reforming of n-octane as a function of H$_2$O/C ratio and temperature.[76] According to this calculation, regions to the right side of the curve should allow stable operation.

Stability maps such as that shown in Figure 7 must be viewed with great caution since kinetics, not thermodynamics, are primarily responsible for stability. For example, the thermodynamic calculations imply that one could steam reform n-octane over a traditional Ni catalyst using an H$_2$O/C ratio of 2 so long as the temperature is above 473 K. However, in our experience, attempts to perform steam reforming using an H$_2$O/C ratio of 2 on Ni catalysts will result in catastrophic formation of carbon for hydrocarbons other than methane.[77] Furthermore, the choice of catalytic materials used for steam reforming strongly affects the parameter space over which materials are stable,[78] showing that one must look more carefully at the mechanism that is responsible for carbon formation in a given system. Finally, the chemical nature of the carbonaceous deposits differs with the catalysts present in the systems.

The formation of carbon over Ni, Fe, and Co has been extensively studied, both for catalytic applications[79-86] and for dusting or dry corrosion, the problem of pitting when steels are exposed to hydrocarbons at high temperatures.[87,88] Recently, the properties of Ni for forming carbon have even been proposed for use in the manufacture of carbon nanofibers.[89,90] The mechanism on each of these metals, shown diagrammatically in Figure 8a, involves deposition of a carbon source onto the metal surface, dissolution of the carbon into the bulk of the metal, and finally precipitation of carbon as a fiber
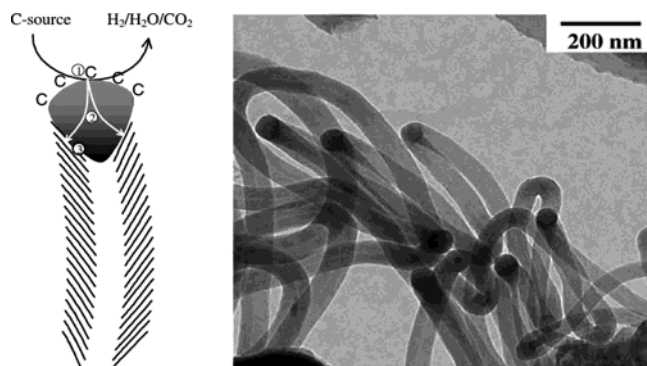
Figure 8. (a) Diagram and (b) microscopy image of carbon formation mechanism from unsupported Ni exposed to 20% C_2H_4/7% H_2 at 823 K. (Reprinted with permission from ref 90. Copyright 2002 Elsevier.)

Figure 9. Temperature programmed oxidation (TPO) data showing CO_2 evolution ($m/e = 44$) of thermally deposited carbon from a Cu-CeO$_2$-YSZ SOFC anode material after exposure to n-butane for 30 min (solid line) and a graphite powder sample (dashed line). (Reprinted with permission from ref 172. Copyright 2003 The Electrochemical Society, Inc.)

at some surface of the metal particle. Figure 8b shows a micrograph of a Ni catalyst that had been exposed to a mixture of C_2H_4 and H_2; the Ni particles are clearly seen at the tips of the carbon filaments. Furthermore, similar filaments were formed from exposure to an Ar-diluted syn-gas feed with a composition of 20% CO and 7% H_2 at 823 K.[90] It is important to recognize that the Ni in Figure 8b is physically lifted from its initial surface and is not merely covered by carbon; this explains the pitting that is observed in dry corrosion. The mechanism also explains why it is necessary to use very high H_2O/C ratios for steam reforming of hydrocarbons larger than methane on Ni catalysts.[91] Filament formation on Ni occurs when carbon deposition onto the Ni surface occurs more rapidly than carbon removal by steam, even if thermodynamic calculations show that carbon will not be stable at equilibrium.

Carbonaceous compounds can also form in the absence of a catalyst by free-radical, gas-phase condensation reactions. The formation of this pyrolytic carbon is known in steam-reforming reactors where it can be controlled to some extent by minimizing the free volume within the reactor chamber.[91] This type of carbon does not form readily with methane but can be severe with larger hydrocarbons. The compounds formed by free-radical reactions tend to be quite different from the graphitic carbon formed by metal catalysts. For example, Lee et al. showed that the compounds formed by passing pure, undi-

luted n-butane over a Cu plate for 24 h at 973 K were soluble in toluene and were primarily polyaromatic,[92] as shown in Table 2. Temperature-programmed oxidation (TPO) measurements performed on Cu−ceria−YSZ composites after exposure to pure n-butane at 973 K for 30 min also indicated that these compounds were easily oxidized as compared to graphite powders. This is shown in Figure 9, where TPO results for the deposits are compared to TPO for graphite.

In addition to the fact that carbon formed by gas-phase pyrolysis is chemically different from that which forms catalytically on Ni, it is important to recognize that carbon formed by pyrolysis forms on the surface rather than in the bulk of the material. Because of this, pyrolysis does not result in pitting of the surfaces to which the hydrocarbon is exposed. Furthermore, on porous Ni cermets, carbon fiber formation can lead to fracture of the electrode caused by the stresses induced by the carbon fibers. Such stresses do not occur upon deposition of pyrolytic carbon.

4. Operation of SOFC on Hydrocarbon Fuels

There are two basic strategies for directly converting hydrocarbons to electrical energy in an SOFC.

Table 2. Chemical Composition of the Carbon Deposit Formed on a Cu Plate after 24 h Exposure to n-Butane at 973 K[a]

name	m/e	no. of aromatic rings
styrene, bicyclo [4,2,0]octa-1.3.5-triene	104	1
ethyl methyl benzene, propenyl benzene etc.	118	1
1,4-dihydronaphthalene	130	1
naphthalene: $C_{10}H_8$	128	2
acenaphthene: $C_{12}H_{10}$	154	2
acenaphthylene: $C_{12}H_8$	152	2
phenanthrene, anthracene: $C_{14}H_{10}$	178	3
2-methy-phenanthrene, 1-methyl-anthracene: $C_{15}H_{12}$	192	3
2-phenylnaphthalene: $C_{16}H_{12}$	204	3
pyrene: $C_{16}H_{10}$	202	4
benzo[a]fluorine, benzo[b]fluorine: $C_{17}H_{12}$	216	3
benzo[a]anthracene, chrysene, triphenylene: $C_{18}H_{12}$	228	4
benzo-pyrene, perylene: $C_{20}H_{12}$	252	5
benzo[ghi]perylene, anthanthrene: $C_{22}H_{12}$	276	6

[a] Reprinted with permission from ref 164. Copyright 2004 The Electrochemical Society, Inc.

The first involves using conventional, Ni-based anodes under conditions in which carbon does not form. This approach necessitates operation in a thermodynamically stable composition and temperature regime but still requires the exercise of caution, given that carbon can form catalytically on Ni surfaces. The second strategy involves using alternative anode materials that do not catalyze carbon formation. Again, caution must be exercised since the cell could be operating under thermodynamically unstable conditions. While most processes of interest do not proceed to thermodynamic equilibrium (or else life itself would be impossible), the high operating temperatures of an SOFC do tend to promote an approach to equilibrium. Furthermore, this second strategy of using alternative materials requires that one avoid catalytic materials on any surface to which the fuel could come into contact, including the bipolar plates and the tubes used to feed the fuel to the anode, not just the anode.

4.1. SOFC with Ni-Based Anodes

At the present time, the most advanced SOFCs are clearly those based on Ni−YSZ, composite anodes. The Ni in these cermet anodes provides electronic conductivity and catalytic activity, both for direct oxidation and for steam reforming of methane. The YSZ provides both ionic conductivity to allow O^{2-} to diffuse farther into the anode and a structural support for the anode that prevents Ni sintering. In some cases, doped ceria is substituted for the YSZ to increase the ionic conductivity.[93−95] In addition to exhibiting excellent electrochemical performance in H_2, Ni cermets are relatively simple to fabricate. For example, tape-calendaring and -casting methods have been developed in which the initial green body is a mixture of NiO and YSZ.[12] Because NiO and YSZ do not form solid solutions, even at high temperatures, this green body can be sintered to form a NiO−YSZ composite and then reduced to form a porous Ni−YSZ cermet. So long as the cermet is approximately 30 vol % Ni,[12] there is sufficient electronic conductivity.

In conventional operation with methane fuels, steam is fed together with the hydrocarbon to promote the steam-reforming reaction and to avoid carbon formation. Because the surface area of Ni in the anode is low, additional catalyst beds are usually included in the anode compartment. In general, only methane can be internally reformed due to the fact that much higher H_2O/C ratios are required for stability with larger hydrocarbons. An important issue with reforming methane in the anode compartment is the fact that steam reforming is strongly endothermic. This can help to remove some of the heat generated by cell inefficiencies, but it can also make it difficult to control the system because of cold spots in the cell, which in turn lead to lower performance on certain parts of the anode. Therefore, some of the reforming is carried out before sending the fuel into the anode compartment. Because operation of conventional SOFC with methane has been discussed in detail elsewhere, we refer the interested reader to several other reviews to learn more about the subject.[96−98]

Barnett and co-workers recently reported that it might be possible to utilize hydrocarbons directly in SOFC with Ni-based anodes.[94,99−102] First, with methane, they observed that there is a narrow temperature window, between ∼550 and 650 °C, in which carbon is not as stable. The equilibrium constant for methane dissociation to carbon and H_2 is strongly shifted to methane below 650 °C, and the equilibrium constant for the Boudouard reaction, the disproportionation of CO to carbon and CO_2, is shifted to CO above 550 °C.[99] Therefore, in this temperature range, they reported that it is possible to operate the cell in a stable manner. (However, a subsequent report by this group showed that there is no stable operating window for ethane due to the fact that carbon formation from ethane is shifted to lower temperatures.[100]) In more recent work, this group has suggested that, even when carbon does form on Ni-based anodes, it may be possible to remove this carbon as fast as it forms if the O^{2-} flux from the electrolyte is sufficient to remove carbon faster than it is formed.[94,100,101] Observations by Weber et al. have confirmed the possibility of stable operation in methane.[103] Similarly, Kendall et al.[104] showed that dilution of methane with CO_2 caused a shift in the reaction mechanism that allowed for more stable operation.

While we acknowledge that the results with methane on Ni cermets are scientifically interesting and that it may be possible to operate a fuel cell with hydrocarbon fuels using Ni-based anodes and low steam contents in a laboratory environment, we do not believe this approach is practical. First, the problem of carbon fiber formation is catastrophic if control of the system is lost. In experiments performed in our laboratory, the effect of exposing a Ni−YSZ cermet to dry methane at 1073 K for 1.5 h resulted in complete destruction of the cermet, with carbon formation equal to several times the weight of the Ni cermet and fracture of the cermet and attached electrolyte layer.[105] Therefore, if it were necessary to operate in a very narrow temperature window to maintain stability, any temperature excursions in the stack, such as might occur during increased loading, would be unacceptable.

Second, it is not possible to prevent carbon formation by a high O^{2-} flux through the electrolyte. O^{2-} can only be responsible for carbon removal in the region near the three-phase boundary, a region that extends no more than approximately 10 μm from the electrolyte interface. This implies that the O^{2-} flux can have no influence on the majority of the Ni cermet, so that the protection afforded the anode through high cell performance is strictly due to the generation of steam or CO_2. While it may be possible to maintain reasonable conversions and high steam concentrations over small-scale, laboratory cells, this will be much harder to do with larger cells, where the conversion at the fuel entrance to the cell will be low. Indeed, the published work with dry methane on Ni cermets has observed significant carbon formation for cells operated at open circuit[101] and anode delamination near the entrance of larger cells.[103]

Finally, an additional approach to using hydrocarbon fuels with Ni-based anodes involves using methanol and ethanol, molecules that carry sufficient oxygen to avoid carbon formation.[106] Unlike the case with low-temperature fuel cells, methanol crossover is not an issue with ceramic membranes. Since methanol decomposes very readily to CO and H_2, SOFC can operate with a very high performance using this fuel.[106,107] In addition, recent work has shown promising performance levels with limited carbon deposition using dimethyl ether as fuel.[108,109]

4.2. Ceramic Anodes

The usual approach to choosing materials for SOFC anodes that will be operated with hydrocarbon fuels is to look first at materials that are good reforming catalysts. Indeed, Ni is one of the best steam-reforming catalysts and is used commercially for that application.[110] Fe and Co have been considered as replacements for Ni since these metals, too, are excellent reforming catalysts. Unfortunately, the same properties that make these metals good reforming catalysts also make them excellent catalysts for the formation of carbon. Therefore, to avoid this problem and operate in hydrocarbon fuels without extensive reforming, it is probably necessary to take a different approach and look at electronically conductive materials that are not good reforming catalysts.

Electronically conductive metal oxides are particularly attractive for this application. Metal oxides tend to be poor reforming catalysts; and, unless reduced to their respective metals, unlikely to form carbon fibers by the mechanism discussed in Section 3. Because they can have very high melting temperatures and relatively low surface energies, oxides tend to be resistant to sintering as compared to metals and could retain anode porosity under extreme conditions. Some oxides exhibit both electronic and ionic conductivity. High ionic conductivity can improve electrode performance by enhancing the size of the TPB, as clearly demonstrated by work on cathode materials.[111-116] Finally, with conductive oxides, it is feasible that the electrode could be a single material, rather than a composite of two or more materials.[117] The potential for solid-state reactions and thermal mismatch problems makes the single component electrode attractive.

Ceria, particularly when doped with Gd_2O_3 or Sm_2O_3,[118-122] has received some attention for direct hydrocarbon conversion in SOFC. Dating back to Steele and co-workers,[123] interesting properties have been demonstrated for ceria-based anodes in direct utilization of methane. Later work suggested that the performance of ceria-based anodes in hydrocarbons could be improved by the addition of precious-metal catalysts, at dopant levels,[124] but the performance of these cells was still too low for practical considerations. The problem with doped ceria is likely that its electronic conductivity is not sufficient. In general, the electrode material should have a conductivity greater than 1 S/cm in order to be practical since a conductivity of 1 S/cm would lead to a cell resistance of 0.1 Ω cm^2 for an electrode thickness of 1 mm, even
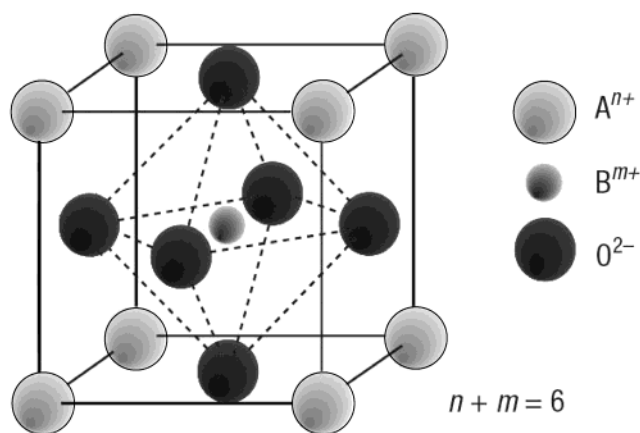
Figure 10. Unit cell of ABO_3 perovskite structure. (Reprinted with permission from *Nature Materials* (http://www.nature.com/nmat), ref 128. Copyright 2003 Nature Publishing Group.)

if the electrode were not porous but dense and no other loss mechanisms were operative within the electrode. At 1073 K, the conductivity of Gd-doped ceria is only 0.08 S/cm.[118]

It is interesting to notice that Marina and co-workers reported excellent performance using a Gd-doped ceria (GDC) anode.[125] At 1000 °C, these investigators reported an anode ASR of 0.39 Ω cm^2 and indicated that they found no carbon deposition with methane using an H_2O/C ratio as low as 0.3 after 1000 h. (The lack of carbon formation is noteworthy since thermodynamic calculations indicate that carbon should be stable under these conditions,[74,75] another indication that carbon formation is related more to kinetic than to thermodynamic considerations.) However, the high performance achieved in this study was almost certainly due to the fact that the GDC anode thickness was between 10 and 15 μm. This implies that the current collector in the cell, a mixture of Au and GDC in this case, becomes even more crucial than usual. One could also argue that this anode is essentially an Au-GDC composite, with Au providing the electronic conduction. Higher electronic conductivities can be obtained in metal oxides having the perovskite structure; the standard materials used for SOFC cathodes, such as LSM, are of this class. For cathode applications, the electrode material must have high electronic conductivity under oxidizing atmospheres, quite different from that experienced in the anode chamber. However, oxides with the perovskite structure can be tailored considerably to achieve the desired properties.[126-128] Perovskites with the general formula ABO_3, where A and B are cations with a total charge of +6, have the unit cell shown in Figure 10. The lower valence A cations are larger and reside on the 6-fold coordinated corners of a simple cubic lattice, with the B cations occupying the 12-fold coordinated center site. The oxygen atoms are found in a face-centered structure around the central B cation.

The perovskite structure is stable to relatively large amounts of dopant ions on either A or B sites. Oxygen vacancies are introduced into the lattice, either through transition-metal redox processes or by doping on the A or B sites with lower valence cations.

Doping of the lattice can alter the structural stability, catalytic activity, and ionic and electronic conductivities of the perovskite. For example, at oxygen contents just below stoichiometry, A-site doped perovskites of the form $La_{1-x}Sr_xFeO_3$ show p-type conductivity. This is due to the Sr-induced charge deficiency being balanced by oxygen vacancies, and relative to the neutral lattice, positively charged Fe ions. At low oxygen activity, the mechanism is n-type as the Fe ions are reduced. There are numerous reviews in the literature presenting a more detailed discussion of perovskite material properties.[129-131]

For application as SOFC anodes, the perovskite must be capable of catalyzing the hydrocarbon oxidation reactions while maintaining high electronic conductivity and structural stability in the highly reducing environment. There have been a number of studies to investigate the stability of various perovskites for this application.[132,133] For example, materials based on doped $LaCrO_3$ were reported to be quite stable.[134] Depending on the dopant, degradation can occur due to reaction with YSZ, due to reduction of the oxide, or due to electrochemical demixing;[135] however, it was reported that, for this material, degradation can be slow even when the oxide is thermodynamically unstable. Furthermore, while many perovskite oxides would not be stable in the anode environment, there are certainly other materials that would be.

The catalytic activities of some perovskites for methane oxidation and steam reforming have also been studied, and it appears that the activity of some materials can be reasonably attractive.[136-143] Considering again materials based on $LaCrO_3$, steam-reforming and methane oxidative-coupling activities have been shown to depend strongly on the dopant ion.[141] Materials doped with Ni gave particularly high steam-reforming activities with lower propensity for carbon formation as compared to a normal Ni catalyst. However, it should be noted that the steam-reforming activity of these materials was reported to be due to reduction and removal of the Ni from the perovskite lattice, a potential source of carbon formation for SOFC anodes operating with dry hydrocarbons. The catalytic properties are also dependent on the oxidation state of the perovskite. For example, Baker et al.[136] and Metcalfe and Baker[137] showed that methane oxidation activities over $La_{0.8}Ca_{0.2}CrO_3$ depended on whether the perovskite had been oxidized or reduced. Methane oxidation to CO_2 was the dominant reaction over a preoxidized sample, but dissociation to carbon and hydrogen occurred once the sample was sufficiently reduced. The presence of easily accessible surface oxygen was suggested as the reason for the change in reaction mechanism.

As with doped ceria, low electronic conductivity is an issue with perovskite anodes as well. Some perovskites show very high electronic conductivities under oxidizing environments, but most of these materials are much less conductive under the reducing environments to which they will be exposed at the anode. For example, the conductivity of $La_{0.75}$-$Sr_{0.25}Cr_{0.5}Mn_{0.5}O_3$, a promising material developed by Tao and Irvine,[117] decreases by almost 2 orders of
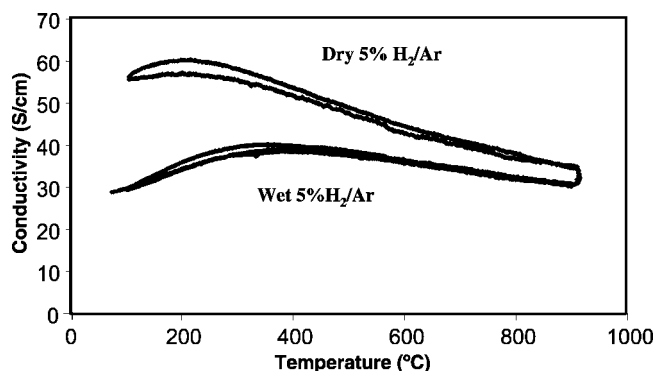
Figure 11. Plot of conductivity vs temperature for $La_2Sr_4Ti_6O_{19-\delta}$ in dry and wet 5%H_2/Ar. (Reprinted with permission from ref 145. Copyright 2003 Elsevier.)

magnitude at 1000 K when the environment changes from air to 5% H_2. An intriguing exception to this is La-doped $SrTiO_3$.[144] Recent reports indicate that this material can exhibit conductivities as high as 500 S/cm at 1273 K when it has been reduced at very high temperatures.[144] Unfortunately, these high conductivities appear to be unstable, decreasing irreversibly after exposure to $P(O_2)$ levels that are typical of those found in the SOFC anode compartment.[144,145] Figure 11, which shows the conductivity of $La_2Sr_4Ti_6O_{19-\delta}$ as a function of temperature in dry and humidified (3%H_2O) 5% H_2/Ar, demonstrates this loss in conductivity with even very low water contents.

Even when exposed to water, the conductivity of the doped $SrTiO_3$ at 973 K, 35 S/cm, would seem to be adequate for achieving good anode performance. However, it should be recognized that a high-performance anode will need to be porous and likely be in the form of a composite with an ionic-conducting oxide to enhance the TPB. For example, with cathodes based on Sr-doped $LaMnO_3$ (LSM) and YSZ, the conductivity of the composite can be more than a factor of 10 lower than that of dense LSM.[146] Furthermore, the intrinsic conductivity of these oxides that are used for cathodes is well over 100 S/cm.

The previous discussion has focused on the properties of perovskite materials rather than on their performance as anodes. The number of actual fuel-cell studies is more limited, but this literature has been reviewed recently by Irvine.[147] Various perovskites have been investigated as potential SOFC anode materials; however, these early efforts were hampered by low electrochemical activity toward methane oxidation,[143,148] poor anode structure,[144] or insufficient electrode conductivity.[45] Most recently, Tao and Irvine[117] demonstrated that an anode based on $(La_{0.75}Sr_{0.25})_{0.9}Cr_{0.5}Mn_{0.5}O_3$ can provide reasonable power densities at 1173 K in 3% humidified CH_4. Barnett and co-workers also reported stable power generation with methane and propane fuels on an anode based on $LaCrO_3$;[94] however, they reported that the addition of Ni, in levels too small to affect the conductivity, was crucial in providing activity for the electrochemical oxidation reactions.

Finally, a number of other mixed oxides that do not have the perovskite structure have also been examined. For example, niobium titanates with the rutile structure,[150] tetragonal tungsten bronze

$(Sr_{1-x}Ba_x)_{0.6}Ti_{0.2}Nb_{0.8}O_{3-}$ phases,[151,152] and yttria−titania zirconates[153,154] have been investigated. All of these materials are likely to be stable for direct hydrocarbon utilization, but none has shown adequate performance for reasons similar to those outlined for the other oxides.

5. Copper-Based Anodes

Another solution to avoiding the coking problems associated with Ni-based anodes is to simply replace the Ni with a metal that is not a catalyst for carbon formation. Metals generally have much higher electronic conductivities than do oxides, so that this problem with ceramic anodes can be circumvented. Unfortunately, there is no metal replacement for Ni that has perfect properties, so that it is necessary to make compromises based on the other performance requirements to select the replacement for Ni. First, the metal must be stable, both to the high operating temperatures and to the range of $P(O_2)$ experienced in the anode. Metals with low melting temperatures are excluded, as are metals such as Mo that would be oxidized by water in the anode compartment. Second, because the metals must be present in quantities sufficient to provide electronic conductivity, precious metals are excluded because of cost.

In our laboratory, we have focused on replacing Ni with Cu. Cu does not catalyze carbon formation and is stable to higher $P(O_2)$ than is Ni. The disadvantages of Cu are that Cu and its oxides have relatively low melting temperatures: 1356 K for Cu, 1508 K for Cu_2O, and 1600 K for CuO. The low melting temperatures for the oxides, in particular, make the fabrication procedures typically used for Ni-cermets inapplicable. Finally, because Cu is not a good oxidation catalyst, we have found that it is necessary to incorporate a separate oxidation catalyst into the anode to achieve a reasonable performance. Because we believe that the problems associated with Cu-based anodes can be overcome and that Cu cermets show great promise for direct-utilization SOFC, the remainder of this review will focus on these materials.

5.1. Preparation Methods

The most commonly used method for producing Ni−cermet anodes starts by simply mixing NiO and the electrolyte (e.g., YSZ) powders. These mixtures can be screen printed onto the electrolyte for electrolyte-supported cells, or for anode-supported cells, the mixtures can be made into plates by pressing, tape-casting, or tape-calendaring.[12] The oxide composites are then heated to a temperature that is sufficient to allow the electrolyte powder in the electrode to become sintered together with the electrolyte. After this high-temperature sintering, the NiO is reduced to Ni by heating in H_2.

Unfortunately, it appears that this method cannot be applied to the fabrication of Cu cermets due to the low melting temperatures of CuO and Cu_2O. For lower sintering temperatures, it is likely that the electrolyte powder within the electrode does not become connected, either to itself or to the electrolyte.
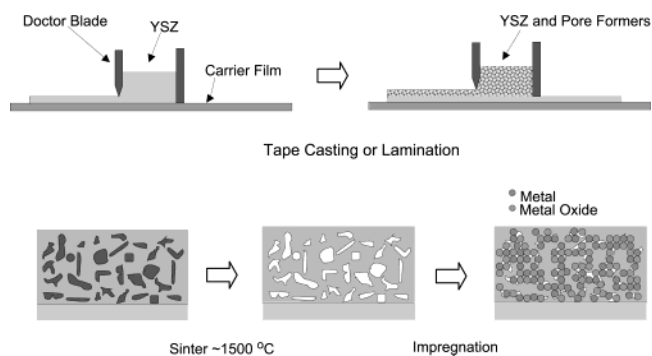
Figure 12. Schematic of SOFC manufacture by tape-casting. (Reprinted with permission from ref 159. Copyright 2000 Wiley-VCH.)

There are indications that these poorly sintered materials are unstable upon reduction of the copper oxides. Two separate studies, one with Cu−YZT[155] and the other with Cu−GDC,[156] have found that the Cu migrates out of the porous electrolyte matrix during reduction.

To avoid these problems, we developed several novel fabrication methods in which the porous oxide component of the cermet is prepared first with additional components added in separate steps that do not require high-temperature processing. In our early work, the porous oxide was prepared from YSZ fibers, stabilized with a zircon coating, supported on relatively thick YSZ electrolyte plates.[157,158] A glycerol slurry of the fibers and normal YSZ powder was applied to the YSZ electrolyte and calcined to high temperatures to form a porous matrix. The matrix was then impregnated with aqueous solutions of nitrate salts, heated to 723 K to decompose the nitrate, and finally reduced in H_2 at the operating conditions to form the anode composite. However, this method does not allow for the fabrication of anode-supported, thin electrolytes, which are required to achieve high performance.

A second method for establishing a porous oxide matrix into which a wide variety of materials can be impregnated involves dual tape-casting, as shown schematically in Figure 12.[159] In tape-casting, oxide powders are mixed together with binders and surfactants and then spread into a film over a carrier such as Mylar.[160] Upon calcination, the binders are burned out, and the oxide particles are sintered to form dense structures. Pore formers, such as graphite or cellulose, can be added to the green tape to introduce a controlled level of porosity. In dual tape casting, a second layer, which could have a different composition, is spread onto the first green layer. In the case shown in Figure 12, graphite pore formers were added to the second layer to achieve porosity after calcination but not to the first. Since the porous layer can be thick and mechanically strong, the dense electrolyte layer can be very thin. Also, pore formers can be added equally well to pressed powders as to tapes. Notice that this methodology can be applied to other electrolyte materials, such as Sm-doped ceria (SDC).[161]

The shape of the pores in the porous oxide matrix can be controlled quite effectively through the shape of the pore formers that are used.[162] Figure 13 shows
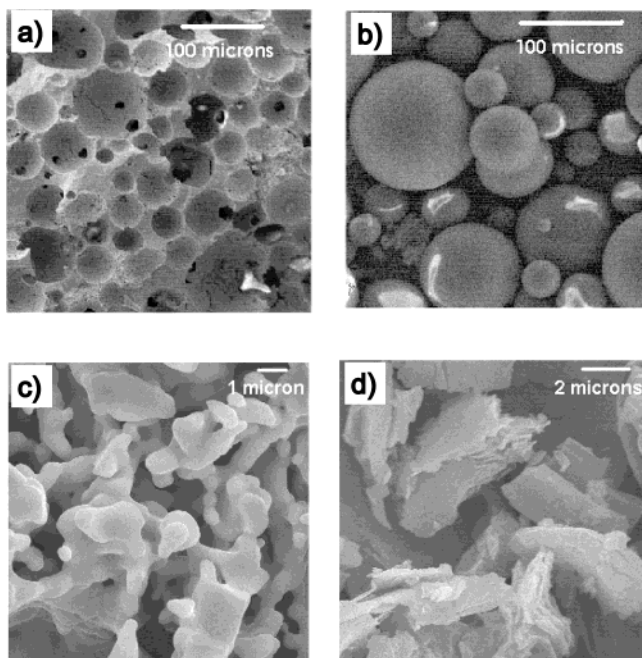
Figure 13. SEM of (a) YSZ ceramic made with 36 wt % PMMA and (b) the PMMA spheres used. (c) YSZ ceramic made with 36 wt % graphite and (d) the graphite particles used. (Reprinted with permission from ref 162. Copyright 2003 The American Ceramic Society (http://www.ceramics.org).)

scanning electron micrographs (SEM) of two ceramic pieces made from YSZ with polymethyl methacrylate (PMMA) or graphite pore formers, along with images of the pore formers themselves. The data are especially clear for PMMA, where the spherical pore formers lead to spherical cavities in the ceramic. The correspondence between cavity and pore-former shape is less clear with graphite, but the size of the pores in the resulting ceramic is certainly similar to the size of the graphite particles. It is interesting to notice that the pore formers leave the ceramic piece at a temperature well below the temperature at which the tape begins to shrink.[162] For example, with PMMA, the pore former had been completely removed by 700 K, while the tape began to shrink only above 1300 K. This helps to explain why the sizes of the cavities in the ceramic piece are somewhat smaller than the size of the pore formers. Obviously, the structure of the pore formers is built into the ceramic at low temperatures, well before most densification occurs, and the pores then shrink at the higher temperatures.

A variation on this dual-tape-casting method involves making a NiO−YSZ composite with a thin YSZ electrolyte in the same manner that is used to make a normal, anode-supported electrolyte with Ni−YSZ cermets.[162,163] After reduction of NiO, the Ni can be leached out of the YSZ using boiling nitric acid, leaving a dense YSZ layer supported on the porous YSZ substrate. SEM pictures of porous YSZ prepared by leaching Ni from Ni−YSZ cermets are shown in Figure 14. In a manner similar to that for PMMA and graphite pore formers (Figure 13) the pore structure of these materials may be controlled by the size and shape of the NiO powder used. The porosity of a typical sample was estimated to be 77% by Hg
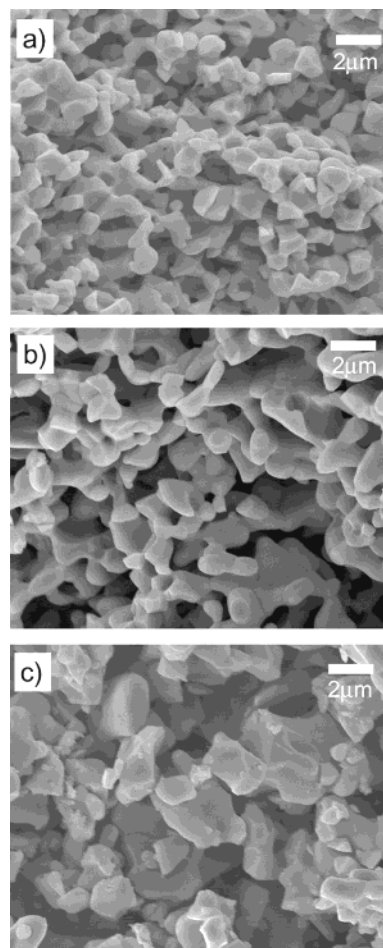
Figure 14. SEM micrographs of porous YSZ produced by acid leaching NiO/YSZ composites. The YSZ had an average particle size of 0.58 μm and the NiO average particle size of (a) 1.2, (b) 4.3, and (c) 17 μm. (Reprinted with permission from ref 162. Copyright 2003 The American Ceramic Society (http://www.ceramics.org).)

porosimetry, and a fairly narrow pore-size distribution between 2 and 4 μm can be achieved.

While it is likely that other methods for preparing Cu cermets will be devised, the materials prepared by dual-tape-casting have some very attractive features. Obviously, the oxide component is very well-connected because it has been sintered at high temperatures. Furthermore, the anode pore structure can be easily tailored by varying the pore former type and quantity. Perhaps of greater significance is the flexibility in anode composition that this high-temperature sintering/low-temperature processing methodology provides. Low-temperature processing allows incorporation of a wide range of catalytic and metallic components by avoiding solid-state reactions. In addition, the surface area and activity of the catalytic material may be preserved. This ability to add a wide variety of materials will be shown to be very important in subsequent sections.

Furthermore, because the Cu is added after the oxide matrix has been established, the structure of the composite is clearly not random; therefore, less metal should be necessary for achieving high electronic conductivities.[164] Figure 15 shows the conductivity of porous YSZ slabs as a function of Cu content in H_2 at 973 K. The porous YSZ was formed using
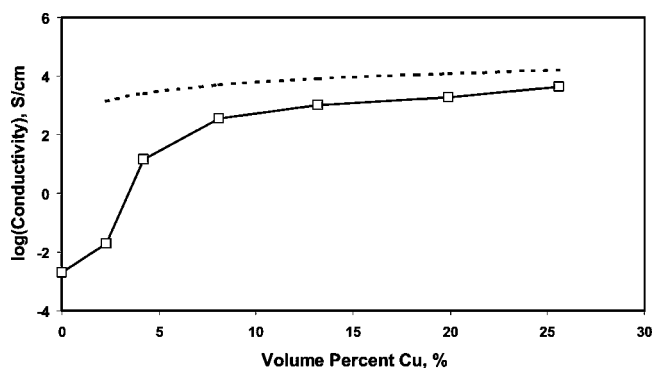
Figure 15. Conductivity as a function of copper content in a porous YSZ slab at 973 K in H_2. The dashed line shows the conductivity predicted for the formation of a thin copper film. (Reprinted with permission from ref 164. Copyright 2004 The Electrochemical Society, Inc.)

graphite pore formers, and the Cu was added by impregnation with aqueous solutions of $Cu(NO_3)_2$, followed by calcination in air at 723 K and reduction in H_2 at 973 K. The conductivity was measured by the four-probe technique. As shown in the figure, the effective conductivity increases dramatically with the addition of relatively small amounts of Cu. The conductivity is 14 S/cm at 4 vol % (11 wt %) Cu and reaches a value of almost 4000 S/cm for 26 vol % (43 wt %). These values are lower than one would predict assuming Cu formed a continuous thin film over the surface of the YSZ; the dashed line in Figure 15 was calculated from the bulk conductivity of Cu, assuming that Cu simply coats the YSZ pores. Obviously, the difference between the measured and calculated values is due to the fact that Cu forms particles that are not necessarily connected. The relationship between conductivity and Cu content for the cermets in this study is very different from that found in earlier studies of more conventional Ni−YSZ[12] and Cu−YZT[155] cermets, where a sharp jump in conductivity is observed at a percolation threshold, near 30 vol % metal.

5.2. Catalysis

The catalytic activity of the anode toward oxidation reactions is a dominant factor in determining SOFC performance, particularly with hydrocarbon fuels. In Cu−cermet anodes, the only role played by Cu is that of electronic conductor. The Cu does not appear to have any catalytic function, and the oxidation reaction in the TPB relies on the addition of other components, primarily ceria.[157−159,165] The evidence for this is as follows. First, Cu−YSZ anodes that do not contain ceria exhibit very low performance, even though they are stable in hydrocarbon fuels.[157−159] Second, substitution of Cu with Au has essentially no effect on anode performance.[166] Since Au is usually thought to be catalytically inert, it seems unlikely that Cu and Au would perform in a similar manner if Cu had a catalytic function.

Other evidence for the importance of catalysis in anode performance came from an examination of the products formed by Cu−ceria−YSZ and Cu−molybdena−YSZ anodes in membrane−reactor measurements.[165] The anodes in these experiments both had
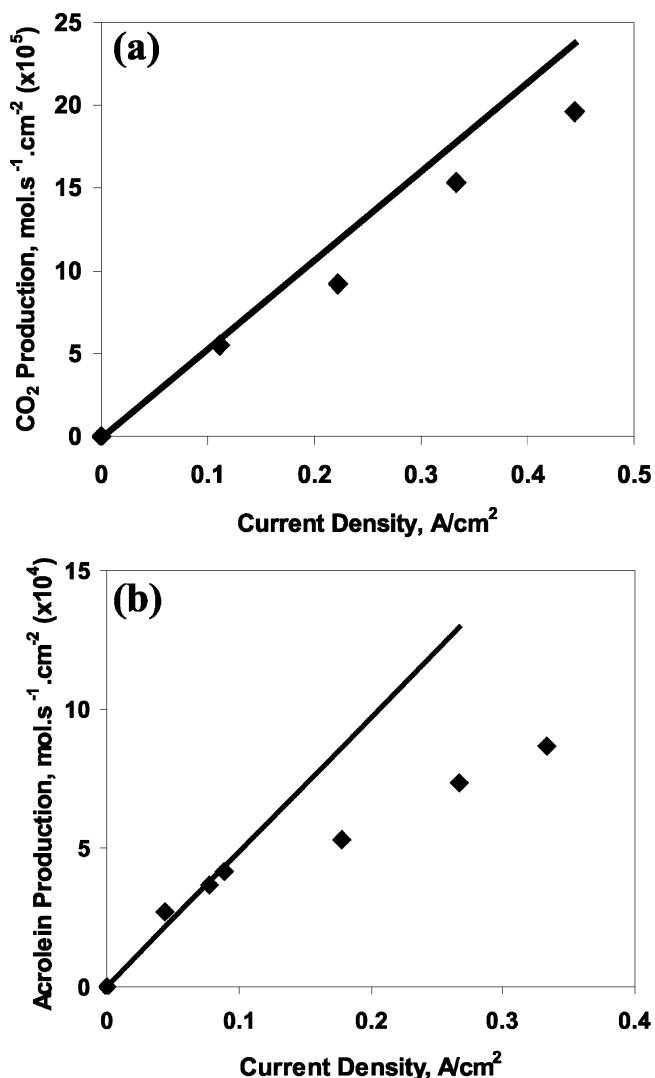
Figure 16. Propylene conversion and product-selectivity results for the membrane-reactor measurements performed at 723 K with pure propylene as the feed. The results in panel a were for the SOFC with a Cu−ceria−YSZ anode, and the results in panel b were for the Cu-molybdena-YSZ anode. In panel a, the points are the rate of CO_2 production, and the line was calculated from the current density and eq 8. In panel b, the points show the production of acrolein, and the line was calculated from eq 9. (Reprinted with permission from ref 165. Copyright 2002 Elsevier.)

20 wt % Cu and 10 wt % added oxide and were identical except for the composition of the added oxide. A power supply was used to fix the potential across the electrodes, while pure propylene was fed to the cells at a temperature of 723 K. The products leaving the anodes were then analyzed as a function of the current density using a gas chromatograph. Results for the Cu−ceria−YSZ anode are shown in Figure 16a. The conversion of propylene at open circuit was negligible but increased almost linearly with the current density. The points shown in the figure are the CO_2 production rates calculated from the chromatographic analysis, while the line is the predicted CO_2 production rate based on Faraday's equation and the measured current

$$CH_2=CHCH_3 + 9O^{2-} \rightarrow 3CO_2 + 3H_2O + 18e^- \quad (8)$$
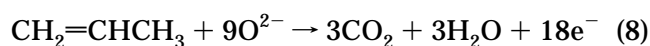
Since only traces of CO were observed and CO_2 and
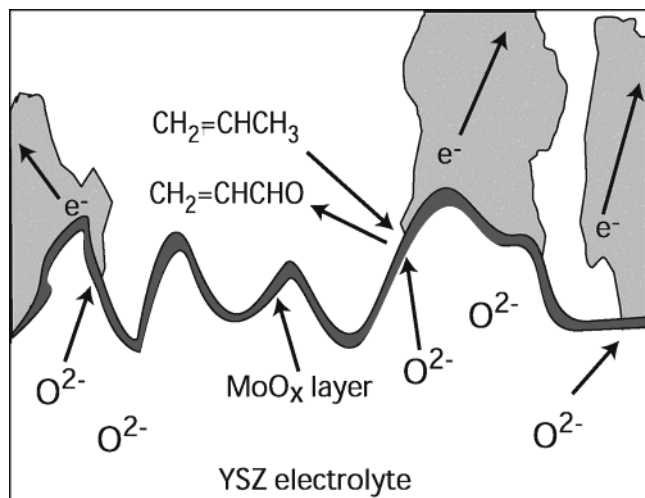
Figure 17. Schematic of anode TPB region during the partial oxidation of propylene. (Reprinted with permission from ref 165. Copyright 2002 Elsevier.)

water were the primary products, the deviation between the line and the points represents a failure to close the mass balance, probably due to an uncertainty in the total flow rate.

Results for the cell with a Cu−molybdena−YSZ anode, shown in Figure 16b, were very different. Unlike ceria, which is a nonselective oxidation catalyst, molybdena is a selective catalyst for the partial oxidation of propylene to acrolein (CH_2=CHCHO) and is used commercially for this process.[167] The primary product at low conversion over the Cu−molybdena−YSZ electrode was acrolein, produced according to the reaction

$$CH_2=CHCH_3 + 2O^{2-} \rightarrow$$
$$CH_2=CHCHO + H_2O + 4e^- \quad (9)$$
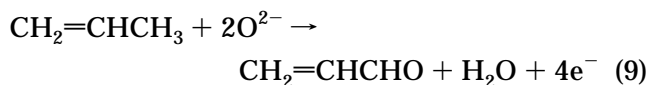
Again, points on the curve were the measured acrolein production rates, and the line is the predicted production rate based on the current and the stoichiometry according to eq 9. At higher conversions, we observed significant amounts of CO_2 and water, sufficient to explain the difference between the acrolein production and the current. It should be noted that others have also observed the electrochemical production of acrolein in a membrane reactor with molybdena in the anode.[166] The selective oxidation of propylene to acrolein with the Cu−molybdena−YSZ anode can only be explained if molybdena is undergoing a redox reaction, presumably being oxidized by the electrolyte and reduced by the fuel. By inference, ceria is also likely acting as a catalyst, but for total oxidation.

The simplest interpretation of these results is that ceria and molybdena act as catalysts in the TPB region, as shown in Figure 17. Either molybdena or ceria are oxidized by O^{2-} coming through the electrolyte and then subsequently reduced by the fuel. According to this picture, reaction at the TPB is a simple redox process with a nonconventional oxygen source. Because molybdena is selective for the oxidation of propylene to acrolein, while ceria is nonselective, the products formed in cells with these two catalysts are different.
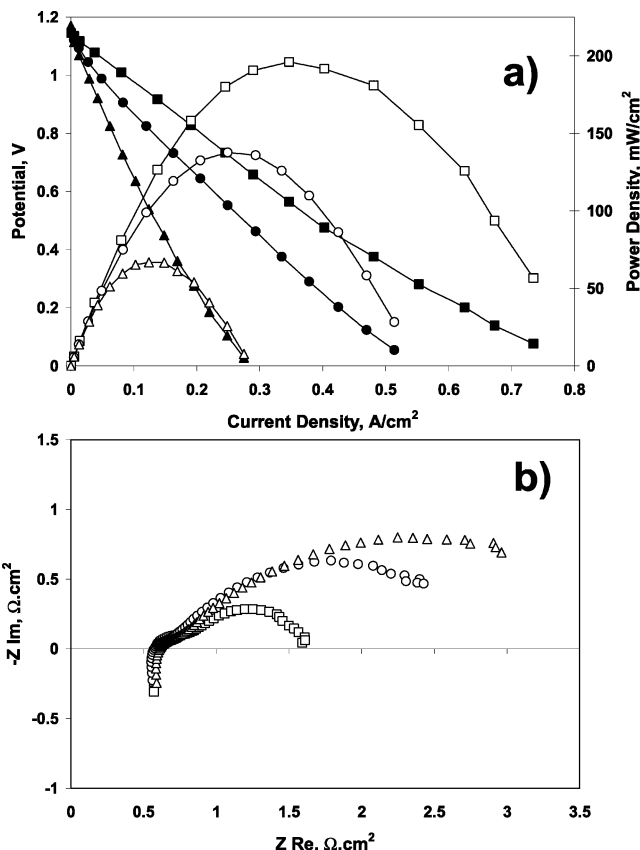
Figure 18. (a) Cell potential (closed symbols) and power density (open symbols) as a function of current density and (b) impedance spectra measured at 330 mA/cm². The cells were calcined for 2 h in air at (□) 723 K, (○) 1273 K, and (△) 1523 K before testing. Measurements were made at 973 K in pure H_2. (Reprinted with permission from ref 169. Copyright 2003 The Electrochemical Society, Inc.)

The anode performance was also found to depend strongly on ceria particle size and morphology, as expected since catalytic properties are crucial.[169] This is demonstrated by the results in Figure 18, which show data for three otherwise identical cells except for the fact that the ceria deposits were calcined in air to either 723, 1273, or 1523 K before the Cu phase was added. While the open-circuit voltage (OCV) on all three cells was in good agreement with the Nernst equation, the maximum power densities decreased with calcination temperature, going from greater than 200 mW/cm² to less than 70 mW/cm² after calcination to 1523 K. Impedance spectra, shown in Figure 18b, demonstrated that the performance changes were due to changes in the anode. In all three cells, the electrolyte resistance was in good agreement with the expected resistance of the YSZ electrolyte. However, the low-frequency (∼4 Hz) arc that can be assigned to the anode increased from 0.8 Ω cm² following calcination at 723 K, to >1.8 Ω cm² at 1273 K and >2.6 Ω cm² at 1523 K. XRD results showed that increasing sintering temperature increased the ceria crystallite size but did not form any new phases within the anode. It is noteworthy that high-temperature calcination of the ceria would have been expected to improve ionic conductivity within the ceria by growth of the ceria crystallites, so that the decreased performance is more likely associated with catalytic properties.
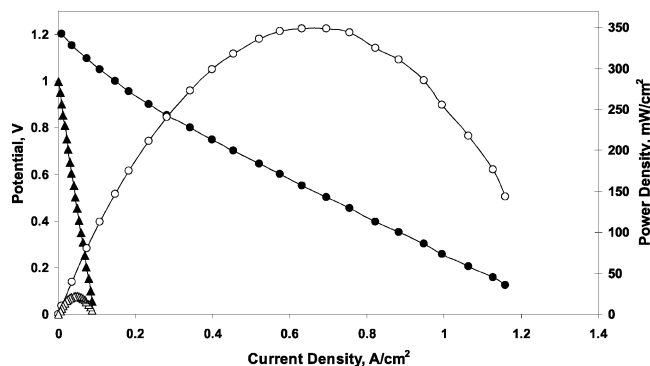
Figure 19. Cell potential (closed symbols) and power density (open symbols) as a function of current density at 973 K in CH_4 for cells with anodes containing (▲) 10% CeO_2 and (●) 10% CeO_2 1% Pd. (Reprinted with permission from ref 60. Copyright 2003 The Electrochemical Society, Inc.)

While ceria is a good hydrocarbon oxidation catalyst, its catalytic activity can be significantly enhanced by the addition of precious metals such as Pt, Pd, and Rh.[60] Unfortunately, cells that contain both Cu and precious metals result in the formation of a catalytically inactive alloy, so that the performance of these cells is essentially indistinguishable from cells made without the addition of precious metals. However, as we will discuss in a subsequent section, electronic conductivity can be obtained in the anode by forming a carbonaceous layer. When electronic conductivity is achieved through carbon deposits, the addition of precious metals at dopant levels into the ceria has a large impact on performance. Figure 19 shows the performance curves in dry methane at 973 K for cells in which the anodes contained 10 wt % CeO_2, with and without the addition of 1 wt % Pd. The addition of Pd increased the power density by greater than 1 order of magnitude, from 22 to 350 mW/cm². The large increase in anode performance is almost certainly associated with enhanced catalytic activity for C−H bond breaking in CH_4.

5.3. Fuel Dependences and Sulfur Tolerance

The performance of SOFCs with Cu−ceria−YSZ anodes has been tested with a wide variety of hydrocarbon fuels, and this has been documented elsewhere.[105,170−171] With the exception of methane, which is known to be relatively unreactive in normal heterogeneous reactions as well, all of the hydrocarbons we examined appear to give similar performance characteristics. The fuels that were tested include n-butane, n-decane, toluene, and a synthetic diesel. The main difference observed between the various fuels is that some fuels tend to form tars more readily via gas-phase free-radical chemistry. Otherwise, with the exception of CH_4, all hydrocarbons that were investigated showed similar power densities. This is shown in Figure 20, which displays the voltage and current densities for n-decane, toluene, and synthetic diesel as a function of time. In this case, the hydrocarbon fuels were diluted in dry N_2 to a concentration of 40 wt % hydrocarbon to prevent condensation of unreacted fuels that leave the cell. (In our studies, the active area for the fuel cell is typically 0.5 cm², and a current density of 1 A/cm² would require a flow
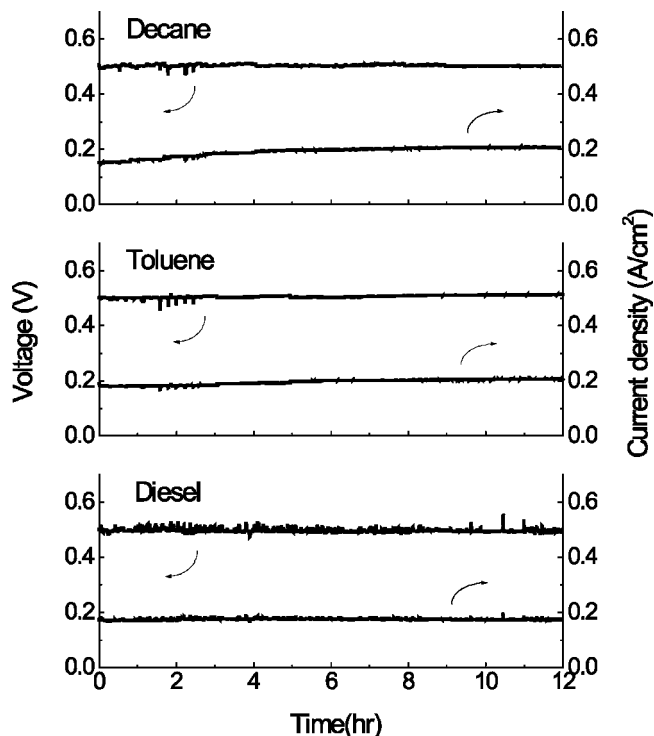
Figure 20. Cell potential and current density as a function of time for n-decane, toluene, and the diesel fuel. Each of the fuels was fed to the cell with N_2 at a concentration of 40 wt % hydrocarbon. (Reprinted with permission from ref 105. Copyright 2001 The Electrochemical Society, Inc.)

rate of only ~0.1 g/h of n-decane at 100% fuel conversion; therefore, the conversions are usually quite low.)

The issue of tar formation is an important one since the anode will obviously cease to function if it becomes filled with tar. In measurements of tar formation rates with n-butane at 973 K, we have recently found that identical amounts of tar are formed on porous YSZ and YSZ with Cu and ceria after 24 h.[172] The fact that the rate of tar deposition is the same whether Cu and ceria are present or not strongly implies that the tar is formed in the gas phase and then deposits onto the anode under operating conditions. Further evidence for gas-phase formation of the tars comes from analysis of the tar by gas chromatography, which showed that the tar consists primarily of polyaromatics with a range of molecular weights[92] since these are the expected products from the gas-phase reaction. Indeed, since many of the gas-phase pyrolysis reactions have been characterized, Walters et al.[173] recently modeled these reactions for light hydrocarbons under SOFC conditions to understand when polyaromatic compounds will likely form and showed that it is only likely to be a problem at the entrance to the fuel cell. However, it is important to notice that gas-phase free-radical reactions are strongly affected by wall effects and that free-radical pyrolysis is routinely minimized in steam-reforming reactors by removing dead volume.[174] Therefore, proper engineering of the flow channels will likely eliminate or at least minimize this problem.

Another issue with hydrocarbon fuels is that essentially all contain some sulfur, and fuel cells can
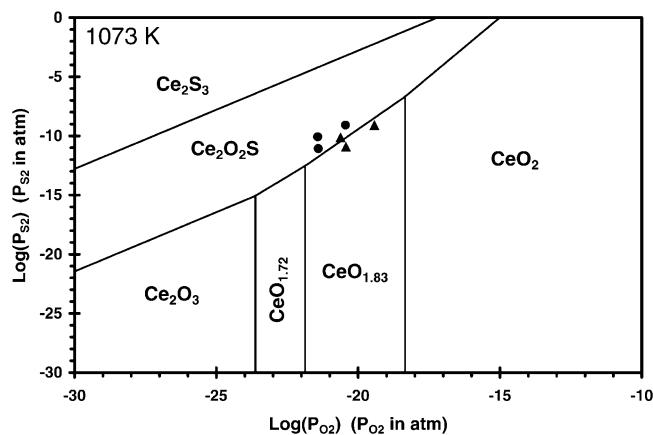
Figure 21. Calculated Ce$-$O$-$S phase diagram at 1073 K. The circles and triangles correspond to conditions for which Ce_2O_2S and cerium oxide were experimentally determined stable. (Reprinted with permission from ref 175. Copyright 2000 Elsevier.)

be very sensitive to even small amounts of sulfur. For example, Ni is used as a getter for H_2S in automotive, emissions-control catalysis, and problems of NiS formation occur in SOFCs. Indeed, the sensitivity of SOFC anodes to sulfur impurities appears to be related to the stability of sulfur compounds that can be formed by the materials in the anodes. In the case of Cu$-$ceria$-$YSZ anodes, the component most sensitive to sulfur is ceria. A phase diagram for the formation of ceria$-$sulfur compounds under reducing conditions is presented in Figure 21. Experimental studies on the formation of Ce$-$O$-$S compounds have shown good agreement with these thermodynamic predictions.[175] Furthermore, conditions that lead to SOFC performance degradation match well with the thermodynamic regime where Ce_2O_2S is predicted to be stable.[176] It is fortunate that reasonably high sulfur concentrations can be used with the Cu$-$ceria$-$YSZ anodes; however, the issue of sulfur sensitivity must be evaluated for any additives that are incorporated in the anode.

5.4. Impact of Fuel Utilization

As discussed in Section 2.4, the Nernst potentials for SOFC operating on hydrocarbons are not as strongly affected by fuel utilization as they are with H_2. However, this advantage is likely to be offset at least somewhat by potential diffusion problems as a result of the dilution that will occur with hydrocarbons. For example, at 50% utilization of n-butane, the fuel concentration will be only 10% due to the fact that 4 mol of CO_2 and 5 mol of H_2O are formed for the oxidation of each mol of n-butane. While we are not aware of any studies with SOFC operating with hydrocarbons at high fuel utilizations, Costas-Nunes et al. simulated the effect of high fuel conversions with n-butane by oxidizing the fuel in pure O_2, either over pure ceria or a Pd/ceria catalyst at 973 K, before admitting it to the anode compartment of the cell.[177] A summary of their results is provided in Figure 22, where the maximum power densities are plotted as a function of fuel conversion using both the ceria and the Pd/ceria catalysts. Figure 22 also shows the maximum power density obtained for
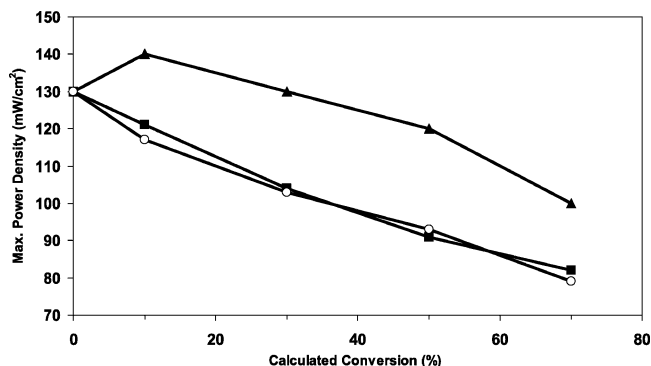
Figure 22. Maximum power density for a Cu-CeO_2-YSZ anode SOFC as a function of the conversion of fuel entering the anode compartment. The data for preoxidation of n-butane by ceria (■) and 1 wt % Pd-ceria (▲) are shown. The maximum power densities obtained when n-butane was diluted with He to a concentration equivalent to that obtained by total oxidation are shown by (○). (Reprinted with permission from ref 177. Copyright 2003 The Electrochemical Society, Inc.)

n-butane that had diluted in He to the same extent as that expected for dilution by CO_2 and H_2O at a particular conversion. It should be noted that the behavior was not diffusion-limited under any of the conditions studied in these cells.

First, it is noteworthy that the maximum power densities obtained with n-butane diluted in He are very similar to those obtained with the cell operating on n-butane preoxidized over a ceria catalyst. Given that chromatographic analysis of the products formed by oxidation over the ceria catalyst showed primarily that CO_2 and H_2O were the products, it appears that CO_2 and H_2O act primarily as diluents for the Cu-based anodes in this study. Obviously, the dilution has a serious impact on performance. However, when n-butane oxidation was carried out over a Pd-ceria catalyst, which is known to be very active for steam reforming,[77] the cell performance was much higher for a given fuel utilization. Chromatographic analysis showed that the increased performance was due to the formation of significant amounts of H_2 generated by steam reforming of n-butane with the steam generated by hydrocarbon oxidation. The maximum power density generated by the cell was as much as 30% with the addition of a reforming component within the oxidation catalyst. On the basis of these results, it is suggested that the inclusion of a steam-reforming catalyst within the anode compartment of direct-conversion SOFC should improve their performance at high fuel utilization.

5.5. Anodes Based on Alloys

As discussed in previous sections, Cu acts primarily as an electronic conductor within the Cu-based anodes. Because it is a poor catalyst for C$-$H and C$-$C bond scission, it is essential to incorporate an oxidation catalyst, ceria, within the anode. While Ni has many attractive properties, its propensity for catalyzing carbon formation prevents its use in dry hydrocarbons at high temperatures. One approach for enhancing the catalytic properties of Cu and stabilizing the tendency of Ni for forming carbon is to use Cu$-$Ni alloys. Cu$-$Ni alloys have been used

| % Cu | 100 | 90 | 80 | 50 | 0 |
| % Ni | 0 | 10 | 20 | 50 | 100 |
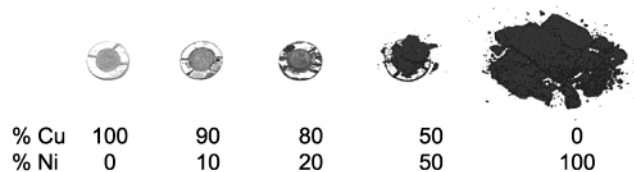
Figure 23. Photographs of cell anodes containing Cu and Ni alloys of varying composition after exposure to dry CH_4 at 1073 K for 1.5 h. (Reprinted with permission from ref 163. Copyright 2002 The Electrochemical Society, Inc.)

for the anodes in molten-carbonate fuel cells in an application where the alloys were found to be more sulfur tolerant as compared to pure Ni.[178]

Using similar methods to make anodes based on Cu−Ni alloys as were used to make the Cu-based cermets, Kim et al.[179] showed that carbon formation on the alloy cermets was significantly suppressed as compared to carbon formation on the pure Ni. This is shown by the picture in Figure 23, in which cermets having various Cu−Ni contents were exposed to dry methane at 1073 K for 1.5 h. The photograph graphically shows that only small amounts of carbon formed on the alloys as compared to what formed on the purely Ni cermet. Using an anode made from $Cu_{0.8}Ni_{0.2}$, they were able to operate the cell for 500 h in dry methane at 1073 K. During that time, the power density continued to rise, up to a value of more than 320 mW/cm^2. The initial poor performance on these alloy anodes appears to have been associated with poor connectivity within the metal phase, with carbon deposits providing that increased conductivity over time. On the basis of this mechanism, one should expect that the initial performance would have been high if more metal had been incorporated within the anode.

The fact that carbon deposited over time on the Cu−Ni alloys is obviously a concern. A later study of anodes based on Cu−Ni alloys found that increasing the reduction temperature from 973 to 1073 K changed the stability of $Cu_{0.8}Ni_{0.2}$ alloys toward carbon formation in the presence of n-butane at 973 K.[180] Cells reduced at 973 K fractured immediately upon exposure to n-butane at this temperature due to the catalytic formation of graphitic carbon, while cells reduced at 1073 K were stable for at least 3 h when exposed to n-butane at 973 K. This indicates that there must be mobility of the two metals at the typical operating temperatures used in the cell. Indeed, previous work on Cu−Ni alloy catalysts has shown that the tendency of the catalyst to form coke is strongly affected if the catalyst is reduced at a temperature greater than 1013 K.[181] While Cu and Ni form solid solutions, it has been found that Ni ensemble size on the surface can be decreased to a minimum size for carbon formation activity with the proper pretreatments.[182] The surface segregation of Cu−Ni alloys is due to Cu having a lower surface energy than Ni,[183] so that the surfaces of Cu−Ni alloys tend to be Cu rich phase. At higher temperatures, the surface concentration of Ni should increase due to entropic effects. However, Ni ensemble size will also decrease for the same reason, which is probably the explanation for the higher stability of Cu−Ni alloys following high-temperature reduction.

Cu−Co mixtures were also investigated for anode cermets and shown to have interesting properties.[180] Cu and Co have a very limited range of compositions where alloys are formed, and diffraction measurements showed that anodes made from mixtures of these two materials had two metal phases. However, mixtures of these metals with Co contents as high as 50 wt % of the metal were stable in n-butane at 973 K for at least 3 h. Since cermets made with 100% Co were not stable to carbon formation under these conditions, it appears that the Co-rich phase must be covered by Cu. There is evidence for surface alloys of Cu and Co, formed because the surface free energy of Cu (1.96 J/m^2) is lower than that of Co (3.23 J/m^2), providing a driving force for Cu to segregate to a Cu−Co surface.[184]

While only a limited amount of testing has been performed on cells made with Cu−Co mixtures, the initial results were intriguing. The addition of even 5% Co to Cu significantly increased the performance of the cells for operation in H_2 at 973 K, from 220 mW/cm^2 on the Cu-based anode to more than 310 mW/cm^2 on the $Cu_{0.95}Co_{0.05}$ anode. A Cu−Co cell also exhibited a power density of 360 mW/cm^2 in pure n-butane at 1073 K, suggesting that bimetallic anodes are worth considering for fuel cells that operate on hydrocarbons.

5.6. Carbon-Based Anodes

Depending on its form, carbon can exhibit reasonably high electronic conductivity. Therefore, one possibility for operating a fuel cell on hydrocarbons is to use carbon itself as the conductor. While relatively little information on this approach is available in the scientific literature, there are indications in the patent literature that this approach has found some success.[185]

At Penn, we have also observed that reasonably high conductivities can be achieved by depositing carbon into a porous YSZ matrix.[164,172] After exposing a porous YSZ matrix to n-butane for 20 h at 973 K, the conductivity was found to increase from 0.002 to 6 S/cm. As discussed in an earlier section, carbon deposits formed by exposure to small hydrocarbons appear to be due to gas-phase, free-radical reactions, with the condensation products depositing only later onto the anode. This is shown by the fact that identical amounts of tar are formed on YSZ substrates, whether Cu or ceria are present. The chemical nature of the carbon deposits has been analyzed using a GC−mass spectrometer, with the results shown in Table 2.[92] These deposits were formed by flowing n-butane over a Cu plate at 973 K. They were then dissolved in toluene before analysis. What the results show is that the molecules are largely polyaromatic compounds that are conductive due to the aromatic ring structure. However, they are clearly not graphitic in nature and can be oxidized at relatively low temperatures as compared to graphite powders.[172]

Anodes using carbon deposits as the conductor can exhibit reasonably high performance. This was shown earlier, in Figure 19, where carbon formed by decomposition of n-butane provided the conductivity
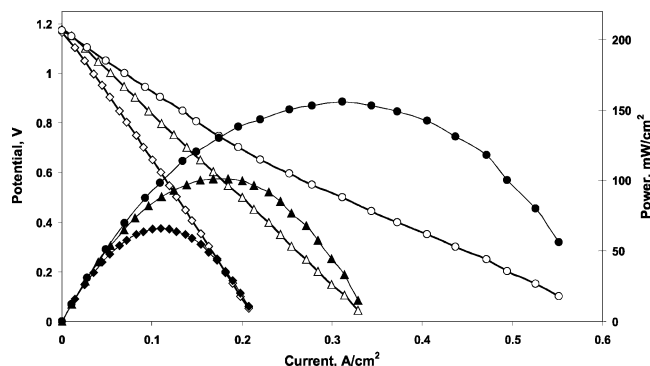
Figure 24. Cell potential (open symbols) and power density (closed symbols) as a function of current for an anode containing 10 wt-% CeO_2 utilizing H_2 fuel at 973 K following 10 min (◆), 1 h (▲), and 24 h (●) exposure to *n*-butane. (Reprinted with permission from ref 164. Copyright 2004 The Electrochemical Society, Inc.)

and Pd and ceria provided the catalytic activity. Figure 24 shows how the conductivity due to carbon evolves with time.[164] In this experiment, the anode was initially a porous, YSZ matrix containing only 10 wt-% CeO_2. Prior to *n*-butane exposure, there was enough conductivity in the anode to achieve an open-circuit voltage (OCV) of 1.16 V, but the maximum power density was a negligible 7 mW/cm². Exposing the anode to *n*-butane for 10 min, 1 h, or 24 h led to increasingly better performance, with the maximum power densities in H_2 at 973 K of 65, 100, and 155 mW/cm², respectively. The primary change in the cell impedance spectra with *n*-butane exposure time was a decrease in the ohmic resistance from 3.86 cm² after 10 min, to 2.20 cm² after 1 h, and 0.71 cm² after 24 h. The nonohmic impedance decreased only slightly with *n*-butane exposure time.

While carbon-containing anodes are scientifically intriguing, it is difficult to see how one could achieve stable performance with these under practical operating conditions. For operation of cells at higher fuel utilization, parts of the anode will be exposed to high steam contents, conditions under which the carbon phases will not be stable.

6. Conclusions

We believe the development of fuel cells that directly utilize hydrocarbon fuels, without the addition of large amounts of steam or air together with the fuel, is a worthwhile and realizable goal. The advantages for using readily available fuels, together with the high intrinsic efficiencies that are possible with fuel cells, are potentially enormous. Admittedly, while great progress has been made toward this development goal, there still are issues that need to be resolved. The reason for our optimism is that, in contrast to the vast literature describing methods for optimizing Ni−cermet anodes, only a very small amount of work has been performed on alternative materials that do not catalyze carbon formation in the way that Ni does. Even so, the performance of cells made with some of these alternative materials is approaching the performance levels achieved by cells with Ni−cermet anodes. While the stability of some of these alternative anodes, especially the Cu-

based systems, toward high temperatures and long operating times has not yet been demonstrated, one should recognize that it is still very early in the development of these materials. As with any new system, novel fabrication methods and the inclusion of promoters and stabilizers should lead to significant improvements. This work is continuing to advance rapidly.

8. References

(1) Armor, J. N. *Appl. Catal. A* **1999** *176*, 159.
(2) Dokiya, M. *Solid State Ionics* **2002** *152*, 383.
(3) Bernay, C.; Marchand, M.; Cassir, M. *J. Power Sources* **2002**, *108*, 139.
(4) Yamada, K.; Takahashi, N.; Wen, C. J. *J. Chem. Eng. Jpn.* **2002**, *35*, 1290.
(5) Williams, M. C.; Strakey, J. P. In *SOFC VIII*; Singhal, S. C., Dokiya, M., Eds.; The Electrochemical Society Proceedings Series PV 2003−07; The Electrochemical Society: Pennington, NJ, 2003; p 3.
(6) Botti, J. J. In *SOFC VIII*; Singhal, S. C., Dokiya, M., Eds.; The Electrochemical Society Proceedings Series PV 2003−07; The Electrochemical Society: Pennington, NJ, 2003; p 16.
(7) Minh, N. In *SOFC VIII*; Singhal, S. C., Dokiya, M., Eds.; The Electrochemical Society Proceedings Series PV 2003−07; The Electrochemical Society: Pennington, NJ, 2003; p 43.
(8) Mukerjee, S.; Shaffer, S.; Zizelman, J. In *SOFC VIII*; Singhal, S. C., Dokiya, M., Eds.; The Electrochemical Society Proceedings Series PV 2003−07; The Electrochemical Society: Pennington, NJ, 2003; p 88.
(9) Petruzzi, L.; Cocchi, S.; Fineschi, F. *J. Power Sources* **2003**, *118*, 96.
(10) Schiller, G.; Henne, R.; Lang, M.; Muller, M. *Mater. Sci. Forum* **2003**, *426-4*, 2539.
(11) Winkler, W.; Lorenz, H. *J. Power Sources* **2002**, *105*, 222.
(12) Minh, N. Q. *J. Am. Ceram. Soc.* **1993**, *76*, 563.
(13) Steele, B. C. H. *Solid State Ionics* **1996**, *86−88*, 1223.
(14) Badwal, S. P. S.; Foger, K. *Ceram. Int.* **1996**, *22*, 257.
(15) Steele, B. C. H. *Philos. Trans. R. Soc. London A* **1996**, *354*, 1695.
(16) Kawada, T.; Yokokawa, H. *Key Eng. Mater.* **1997**, *125−126*, 187.
(17) McEvoy, A. J. *Mater.-wiss. u. Werkstofftech.* **2002**, *33*, 331.
(18) Tietz, F.; Buchkremer, H.-P.; Stöver, D. *Solid State Ionics* **2002**, *152−153*, 373.
(19) Tietz, F. *Mater. Sci. Forum* **2003**, *426−432*, 4465.
(20) Ormerod, R. M. *Chem. Soc. Rev.* **2003**, *32*, 17.
(21) Quadakkers, W. J.; Piron-Abellan, J.; Shemet, V.; Singheiser, L. *Mater. High Temp.* **2003**, *20*, 115.
(22) Brandon, N. P.; Skinner, S.; Steele, B. C. H. *Annu. Rev. Mater. Sci.* **2003**, *33*, 183.
(23) Metcalfe, I. S. *Chem. Eng. Technol.* **2003**, *26*, 857.
(24) Paz, E. E.; Wang, C.; Palanisamy, C.; Gorte, R. J.; Vohs, J. M. In *SOFC VIII*; Singhal, S. C., Dokiya, M., Eds.; The Electrochemical Society Proceedings Series PV 2003−07; The Electrochemical Society: Pennington, NJ, 2003; p 787.
(25) Mogensen, M.; Kammer, K. *Annu. Rev. Mater. Res.* **2003**, *33*, 321.
(26) Marina, O. A.; Mogensen, M. *Appl. Catal. A* **1999**, *189*, 117.
(27) Park, S.; Vohs, J. M.; Gorte, R. J. *Nature* **2000**, *404*, 265.

(28) Craciun, R.; Shereck, B.; Gorte, R. J. *Catal. Lett.* **1998**, *51*, 149.
(29) Fellows, R. *J. Power Sources* **1998**, *71*, 281.
(30) Kortbeek, P. J.; Ottervanger, R. *J. Power Sources* **1998**, *71*, 223.
(31) Stevenson, D. A.; Jiang, N.; Buchanan, R. M.; Henn, F. E. G. *Solid State Ionics* **1993**, *62*, 279.
(32) Nowick, A. S.; Du, Y. *Solid State Ionics* **1995**, *77*, 137.
(33) Zhu, B.; Rundgren, K.; Mellander, B.-K. *Solid State Ionics* **1997**, *97*, 385.
(34) Iwahara, H. *Solid State Ionics* **1999**, *125*, 271.
(35) Corcoran, D. J. D.; Tunstall, D. P.; Irvine, J. T. S. *Solid State Ionics* **2000**, *136*, 297.
(36) Kreuer, K. D. *Annu. Rev. Meter. Res.* **2003**, *33*, 333.
(37) Dees, D. W.; Claar, T. D.; Easler, T. E.; Fee, D. C.; Mrazek, F. C. *J. Electrochem. Soc.* **1987**, *134*, 2141.
(38) George, R. A.; Bessette, N. F. *J. Power Sources* **1998**, *71*, 131.
(39) Casanova, A. *J. Power Sources* **1998**, *71*, 65.
(40) Singhal, S. C. *Solid State Ionics* **2000**, *135*, 305.
(41) Yokokawa, H. *Annu. Rev. Mater. Res.* **2003**, *33*, 581.
(42) Wang, X.; Nakagawa, N.; Kato, K. *J. Electrochem. Soc.* **2001**, *148*, A565.
(43) Horita, T.; Yamaji, K.; Sakai, N.; Xiong, Y.; Kato, T.; Yokokawa, H.; Kawada, T. *J. Power Sources* **2002**, *106*, 224.
(44) Mizusaki, J.; Tagawa, H.; Tsuneyoshi, K.; Sawata, A. *J. Electrochem. Soc.* **1991**, *138*, 1867.
(45) de Haart, L. G. J.; Kuipers, R. A.; de Vries, K. J.; Burggraaf, A. J. *J. Electrochem. Soc.* **1991**, *138*, 1970.
(46) Østergård, M. J. L.; Mogensen, M. *Electrochim. Acta* **1993**, *38*, 2015.
(47) Fukunaga, H.; Ihara, M.; Sakaki, K.; Yamada, K. *Solid State Ionics* **1996**, *86–88*, 1179.
(48) Tanner, C. W.; Fung, K.-Z.; Virkar, A. V. *J. Electrochem. Soc.* **1997**, *22*, 144.
(49) Brown, M.; Primdahl, S.; Mogensen, M. *J. Electrochem. Soc.* **2000**, *475*, 147.
(50) Virkar, A. V.; Fung, K. Z.; Tanner, C. W. U.S. Patent No. 5,-543,239, 1996.
(51) Fleig, J. *J. Power Sources* **2002**, *105*, 228.
(52) Herbstritt, D.; Müller, A. C.; Weber, A.; Ivers-Tiffée, E. In *SOFC VIII*; Singhal, S. C., Dokiya, M., Eds.; The Electrochemical Society Proceedings Series PV 2003–07; The Electrochemical Society: Pennington, NJ, 2003; p 1330.
(53) Kleveland, K.; Einarsrud, M.-A.; Schmidt, C. R.; Shamsili, S.; Faaland, S.; Wiik, K.; Grande, T. *J. Am. Ceram. Soc.* **1999**, *82*, 729.
(54) Colomer, M. T.; Steele, B. C. H.; Kilner, J. A. *Solid State Ionics* **2002**, *147*, 41.
(55) Simner, S. P.; Bonnett, J. F.; Canfield, K. D.; Shelton, J. P.; Sprenkle, V. L.; Stevenson, J. W. *J. Power Sources* **2003**, *113*, 1.
(56) EG&G Technical Services, Inc. *Fuel Cell Handbook 6th Edition*; DOE/NETL-2002/1179; U.S. Department of Energy, Office of Fossil Energy, National Energy Technology Laboratory: Morgantown, WV; p 2.1–2.26
(57) Svensson, A. M.; Sunde, S.; Nisancioglu, K. *Solid State Ionics* **1996**, *86–88*, 1211.
(58) Kim, J.-H.; Virkar, A. V.; Fung, K.-Z.; Mehta, K.; Singhal, S. C. *J. Electrochem. Soc.* **1999**, *146*, 69.
(59) Williford, R. E.; Chick, L. A.; Maupin, G. D.; Simmer, S. P.; Stevenson, J. W. *J. Electrochem. Soc.* **2003**, *150*, A1067.
(60) McIntosh, S.; Vohs, J. M.; Gorte, R. J. *Electrochem. Solid-State Lett.* **2003**, *6*, A240.
(61) Park, S.; Craciun, R.; Vohs, J. M.; Gorte, R. J. *J. Electrochem. Soc.* **1999**, *146*, 3603.
(62) Juhl, M.; Primdahl, S.; Manon, C.; Mogensen M. *J. Power Sources* **1996**, *61* 173.
(63) Murray, E. P.; Barnett, S. A. *Solid State Ionics* **2001**, *143*, 265.
(64) McIntosh, S.; Adler, S. B.; Vohs, J. M.; Gorte, R. J. *Electrochem. Solid-State Lett.* **2004**, *7*, A111.
(65) McIntosh, S.; Vohs, J. M.; Gorte, R. J. *J. Electrochem. Soc.* **2003**, *150*, A1305.
(66) Jiang, S. P.; Love, J. G.; Badwal, S. P. S. *Key Eng. Mater.* **1997**, *125–126*, 81.
(67) Winkler, J.; Hendriksen, P. V.; Bonanos, N.; Moegensen, M. *J. Electrochem. Soc.* **1998**, *145*, 1184.
(68) Figueiredo, F. M.; Frade, J.; Marques, F. M. B. *Bol. Soc. Esp. Cerám. Vidrio* **1999**, *38*, 369.
(69) Adler, S. B.; Henderson, B. T.; Wilson, M. A.; Taylor, D. M.; Richards, R. E. *Solid State Ionics* **2000**, *134*, 35.
(70) Kato, T.; Momma, A.; Kaga, Y.; Nagata, S.; Kasuga, Y.; Kitase, M. *Solid State Ionics* **2000**, *132*, 287.
(71) Chan, S. H.; Chen, X. J.; Khor, K. A. *J. Appl. Electrochem.* **2001**, *31*, 1163.
(72) Takeguchi, T.; Kani, Y.; Yano, T.; Kikuchi, R.; Eguchi, K.; Tsujimoto, K.; Uchida, Y.; Ueno, A.; Omoshiki, K.; Aizawa, M. *J. Power Sources* **2002**, *112*, 588.
(73) Eguchi, K.; Kojo, H.; Takeguchi, T.; Kikuchi, R.; Sasaki, K. *Solid State Ionics* **2002**, *152–153*, 411.
(74) Sasaki, K.; Teraoka, Y. *J. Electrochem. Soc.* **2003**, *150*, A878.
(75) Sasaki, K.; Teraoka, Y. *J. Electrochem. Soc.* **2003**, *150*, A885.
(76) EG&G Technical Services, Inc. *Fuel Cell Handbook 6th Edition*; DOE/NETL-2002/1179; U.S. Department of Energy, Office of Fossil Energy, National Energy Technology Laboratory: Morgantown, WV; p 8–24.
(77) Wang, X.; Gorte, R. J. *Catal. Lett.* **2001**, *73*, 15.
(78) Wang, X.; Gorte, R. J. *App. Catal. A* **2002**, *224*.
(79) Baker, R. T. K.; Barber, M. A.; Harris, P. S.; Feates, F. D.; Waite, R. J. *J. Catal.* **1972**, *26*, 51.
(80) Baker, R. T. K.; Harris, P. S.; Henderson, J.; Thomas, R. B. *Carbon* **1975**, *13*, 17.
(81) Baker, R. T. K.; Harris, P. S.; Terry, S. *Nature* **1975**, *253*, 37.
(82) Keep, C. W.; Baker, R. T. K.; France, J. A. *J. Catal.* **1977**, *47*, 232.
(83) Bartholomew, C. H. *Catal. Rev.—Sci. Eng.* **1982**, *24*, 67.
(84) Baker, R. T. K. *Carbon* **1989**, *27*, 315.
(85) Zhang, T.; Amiridis, M. D. *Appl. Catal. A* **1998**, *167*, 161.
(86) Monnerat, B.; Kiwi-Minsker, L.; Renken, A. *Chem. Eng. Sci.* **2001**, *56*, 633.
(87) Chun, C. M.; Mumford, J. D.; Ramanarayanan, T. A. In *SOFC VI*; Singhal, S. C., Dokiya, M., Eds.; The Electrochemical Society Proceedings Series PV 1999–19; The Electrochemical Society: Pennington, NJ, 1999; p 621.
(88) Toh, C. H.; Munroe, P. R.; Young, D. J.; Foger, K. *Mater. High Temp.* **2003**, *20*, 129.
(89) Chen, P.; Zhang, H.-B.; Lin, G.-D.; Hong, Q.; Tsai, K. R. *Carbon* **1997**, *100–11*, 1495.
(90) Toebes, M. L.; Bitter, J. H.; van Dillen, A. J.; de Jong, K. P. *Catal. Today* **2002**, *76*, 33.
(91) Farrauto, R. J.; Bartholomew, C. H. *Fundamentals of Industrial Catalytic Processes*, 1st ed.; Blackie Academic and Professional: London, 1997; p 351.
(92) Lee, S.-I.; McIntosh, S.; Vohs, J. M.; Gorte, R. J. In *SOFC VIII*; Singhal, S. C., Dokiya, M., Eds.; The Electrochemical Society Proceedings Series PV 2003–07; The Electrochemical Society: Pennington, NJ, 2003; p 865.
(93) Wang, J. B.; Jang, J.-C.; Huang, T.-J. *J. Power Sources* **2003**, *122*, 122.
(94) Liu, J.; Madsen, B. D.; Ji, Z.; Barnett, S. A. *Electrochem. Solid-State Lett.* **2002**, *5*, A122.
(95) Livermore, A. J. A.; Cotton, J. W.; Ormerod, R. M. *J. Power Sources* **2000**, *86*, 411.
(96) Dicks, A. L. *J. Power Sources* **1996**, *61*, 113.
(97) Clarke, A. H.; Dicks, A. L.; Pointon, K.; Smith, T. A.; Swann, A. *Catal. Today* **1997**, *38*, 411.
(98) Dicks, A. L. *J. Power Sources* **1998**, *71*, 111.
(99) Murray, E. P.; Tsai, T.; Barnett, S. A. *Nature* **1999**, *400*, 649.
(100) Murray, E. P.; Barnett, S. A. In *SOFC VI*; Singhal, S. C., Dokiya, M., Eds.; The Electrochemical Society Proceedings Series PV 1999–19; The Electrochemical Society: Pennington, NJ, 1999; p 1001.
(101) Liu, J.; Barnett, S. A. *Solid State Ionics* **2003**, *158*, 11.
(102) Zhan, Z.; Madsen, B. D.; Liu, J.; Barnett, S. A. In *SOFC VIII*; Singhal, S. C., Dokiya, M., Eds.; The Electrochemical Society Proceedings Series PV 2003–07; The Electrochemical Society: Pennington, NJ, 2003; p 1286.
(103) Weber, A.; Sauer, B.; Müller, A. C.; Herbstritt, D.; Ivers-Tiffée, E. *Solid State Ionics* **2002**, *152–153*, 543.
(104) Kendall, K.; Finnerty, C. M.; Saunders, G.; Chung, J. T. *J. Power Sources* **2002**, *106*, 323.
(105) Kim, H.; Park, S.; Vohs, J. M.; Gorte, R. J. *J. Electrochem. Soc.* **2001**, *148*, A693.
(106) Jiang, Y.; Virkar, A. V. *J. Electrochem. Soc* **2001**, *148*, A706.
(107) Saunders, G. J.; Kendall, K. *J. Power Sources* **2002**, *106*, 258.
(108) Wang, S.; Isiharah, T.; Takita, Y. *Electrochem. Solid-State Lett.* **2002**, *5*, A177.
(109) Murray, E. P.; Harris, S. J.; Jen, H. *J. Electrochem. Soc.* **2002**, *149*, A1127.
(110) Farrauto, R. J.; Bartholomew, C. H. *Fundamentals of Industrial Catalytic Processes*, 1st ed.; Blackie Academic and Professional: London, 1997; p 349.
(111) Murray, E. P.; Barnett, S. A. *Solid State Ionics* **2001**, *143*, 265.
(112) Ralph, J. M.; Schoeler, A. C.; Krumpelt, M. *J. Mater. Sci.* **2001**, *36*, 1161.
(113) Hart, N. T.; Brandon, N. P.; Day, M. J.; Lapeña-Rey, N. *J. Power Sources* **2002**, *106*, 42.
(114) Colomer, M. T.; Steele, B. C. H.; Kilner, J. A. *Solid State Ionics* **2002**, *147*, 41.
(115) Simner, S. P.; Bonnett, J. F.; Canfield, N. L.; Meinhardt, K. D.; Shelton, J. P.; Sprenkle, V. L.; Stevenson, J. W. *J. Power Sources* **2003**, *113*, 1.
(116) Huang, Y.; Vohs, J. M.; Gorte, R. J. *J. Electrochem. Soc.* **2004**, *151*, A646.
(117) Tao, S.; Irvine, J. T. S. *Nat. Mat.* **2003**, *2*, 320.
(118) Eguchi, K.; Setoguchi, T.; Inoue, T.; Arai, H. *Solid State Ionics* **1992**, *52*, 165.
(119) Mogensen, M.; Lindegaard, T.; Hansen, U. R.; Mogensen, G. *J. Electrochem. Soc.* **1994**, *141*, 2122.
(120) Eguchi, K. *J. Alloys Compd.* **1997**, *250*, 486.

(121) Mogensen, M.; Sammes, N. M.; Tompsett, G. A. *Solid State Ionics* **2000**, *129*, 63.
(122) Ramírez-Cabrera, E.; Laosiripojana, N.; Atkinson, A.; Chadwick, D. *Catal. Today* **2003**, *78*, 433.
(123) Steele, B. C. H.; Middleton, P. H.; Rudkin, R. A. *Solid State Ionics* **1990**, *40–41*, 388.
(124) Putna, E. S.; Stubenrauch, J.; Vohs, J. M.; Gorte, R. J *Langmuir* **1995**, *11*, 4832.
(125) Marina, O. A.; Bagger, C.; Primdahl, S.; Mogensen, M. *Solid State Ionics* **1999**, *123*, 199.
(126) Bouwmeester, H. J. M.; Burggraaf, A. J. In *The CRC Handbook of Solid State Electrochemistry*; Gellings, P. J., Bouwmeester, H. J. M., Eds.; CRC Press: Boca Raton, FL, 1997; p 481.
(127) Sauvet, A.; Irvine, J. T. S. *Fuel Cells* **2001**, *1*, 205.
(128) Boukamp, B. A *Nat. Mat.* **2003**, *2*, 294.
(129) Andersen, H. U. *Solid State Ionics* **1992**, *52*, 33.
(130) Mizusaki, J. *Solid State Ionics* **1992**, *52*, 79.
(131) van Hassel, B. A.; Kawada, T.; Sakai, N.; Yokokawa, H.; Dokiya, M.; Bouwmeester, H. J. M. *Solid State Ionics* **1993**, *66*, 295.
(132) Yokokawa, H.; Sakai, N.; Kawada, T.; Dokiya, M. *Solid State Ionics* **1992**, *52*, 43.
(133) Xu, S. J.; Thomson, W. J. *Ind. Eng. Chem. Res.* **1998**, *37*, 1290.
(134) Sfeir, J. *J. Power Sources* **2003**, *118*, 276.
(135) Sfeir, J.; van Herle, J.; McEvoy, A. J. *J. Eur. Ceram. Soc.* **1999**, *19*, 897.
(136) Baker, R. T.; Metcalfe, I. S.; Middleton, P. H.; Steele, B. C. H. *Solid State Ionics* **1994**, *72*, 328.
(137) Metcalfe, I. S.; Baker, R. T. *Catal. Today* **1996**, *27*, 285.
(138) Stojanović, M.; Mims, C. A.; Modallal, H.; Yang, Y. L.; Jacobson, A. J. *J. catal.* **1997**, *166*, 324.
(139) Weston, M.; Metcalfe, I. S. *Solid State Ionics* **1998**, *113–115*, 247.
(140) Hartley, A.; Sahibzada, M.; Weston, M.; Metcalfe, M.; Mantzavinos, D. *Catal. Today* **2000**, *55*, 197.
(141) Sfeir, J.; Buffat, P. A.; Möckli, P.; Xanthopoulos, N.; Vasquez, R.; Mathieu, H. J.; van Herle, J.; Thampi, K. R. *J. Catal.* **2001**, *202*, 229.
(142) Kirchnerova, J.; Alifanti, M.; Delmon, B. *Appl. Catal., A* **2002**, *231*, 65.
(143) Alifanti, M.; Auer, R.; Kirchnerova, J.; Thyrion, F.; Grange, P.; Delmon, B. *Appl. Catal. B* **2003**, *41*, 71.
(144) Marina, O. A.; Canfield, N. L.; Stevenson, J. W. *Solid State Ionics* **2002**, *149*, 21.
(145) Canales-Vázquez, J.; Tao, S. W.; Irvine, J. T. S. *Solid State Ionics* **2003**, *159*, 159.
(146) He, H.; Huang, Y.; Regal, J.; Boaro, M.; Vohs, J. M.; Gorte, R. J. *J. Am. Ceram. Soc.* **2004**, *87*, 331.
(147) Irvine, J. T. S.; Sauvet, A. *Fuel Cells* **2001**, *1*, 205.
(148) Primdahl, S.; Hansen, J. R.; Grahl-Madsen, L.; Larsen, P. H. *J. Electrochem. Soc.* **2001**, *148*, A74.
(149) He, H.; Huang, Y.; Vohs, J. M.; Gorte, R. J. *Solid State Ionics*, in press.
(150) Reich, C. M.; Kaiser, A.; Irvine, J. T. S. *Fuel Cells* **2001**, *1*, 249.
(151) Slater, P. R.; Irvine, J. T. S. *Solid State Ionics* **1999**, *120*, 125.
(152) Kaiser, A.; Bradley, J. L.; Slater, P. R.; Irvine, J. T. S. *Solid State Ionics* **2000**, *135*, 519.
(153) Kelaidopoulou, A.; Siddle, A.; Dicks, A. L.; Kaiser, A.; Irvine, J. T. S. *Fuel Cells* **2001**, *1*, 219.
(154) Kelaidopoulou, A.; Siddle, A.; Dicks, A. L.; Kaiser, A.; Irvine, J. T. S. *Fuel Cells* **2001**, *1*, 226.
(155) Kiratzis, N.; Holtappels, P.; Hatchwell, C. E.; Mogensen, M.; Irvine, J. T. S. *Fuel Cells* **2001**, *1*, 211.

(156) Joerger, M. B.; Baeurle, L. M.; Gauckler, L. J. In *Proceedings of the 5th European Solid Oxide Fuel Cell Forum*; Huijsmans, J., Ed.; The European Fuel Cell Forum: Oberrohrdorf, Switzerland, 2002; p 475.
(157) Craciun, R.; Park, S.; Gorte, R. J.; Vohs, J. M.; Wang, C.; Worrell, W. L. *J. Electrochem. Soc.* **1999**, *146*, 4019.
(158) Park, S.; Craciun, R.; Vohs, J. M.; Gorte, R. J. *J. Electrochem. Soc.* **1999**, *146*, 3603.
(159) Gorte, R. J.; Park, S.; Vohs, J. M.; Wang, C. *Adv. Mater.* **2000**, *12*, 1465.
(160) Mistler, R. E.; Twiname, E. R. *Tape Casting: Theory and Practice*; The American Ceramic Society: Westerville, OH, 2002.
(161) Lu, C.; Worrell, W. L.; Gorte, R. J.; Vohs, J. M. *J. Electrochem. Soc.* **2003**, *150*, A354.
(162) Boaro, M.; Vohs, J. M.; Gorte, R. J. *J. Am. Ceram. Soc.* **2003**, *86*, 395.
(163) Kim, H.; da Rosa, C.; Boaro, M.; Vohs, J. M.; Gorte, R. J. *J. Am. Ceram. Soc.* **2002**, *85*, 1473.
(164) McIntosh, S.; He, H.; Lee, S.-I.; Costa-Nunes, O.; Krishnan, V. V.; Vohs, J. M.; Gorte, R. J. *J. Electrochem. Soc.* **2004**, *151*, A604.
(165) McIntosh, S.; Vohs, J. M.; Gorte, R. J. *Electrochim. Acta* **2002**, *47*, 3815.
(166) Lu, C.; Worrell, W. L.; Vohs, J. M.; Gorte, R. J. *J. Electrochem. Soc.* **2003**, *150*, A1357.
(167) Farrauto, R. J.; Bartholomew, C. H. *Fundamentals of Industrial Catalytic Processes*, 1st ed.; Blackie Academic and Professional: London, 1997; p 489.
(168) Stoukides, M. *Catal. Rev. Sci. Eng.* **2000**, *42*, 1.
(169) He, H.; Vohs, J. M.; Gorte, R. J. *J. Electrochem. Soc.* **2003**, *150*, A1470.
(170) Gorte, R. J.; Vohs, J. M. *J. Power Sources* **2002**, *106*, 10.
(171) Gorte, R. J.; Vohs, J. M. *J. Catal.* **2003**, *216*, 477.
(172) McIntosh, S.; Vohs, J. M.; Gorte, R. J. *J. Electrochem. Soc.* **2003**, *150*, A470.
(173) Walters, K. M.; Dean, A. M.; Zhu, H.; Kee, R. J. *J. Power Sources* **2003**, *123*, 182.
(174) Farrauto, R. J.; Bartholomew, C. H. *Fundamentals of Industrial Catalytic Processes*, 1st ed.; Blackie Academic and Professional: London, 1997; p 355.
(175) Ferrizz, R. M.; Gorte, R. J.; Vohs, J. M. *Appl. Catal. B* **2003**, *43*, 273.
(176) Kim, H.; Vohs, J. M.; Gorte, R. J. *Chem. Commun.* **2001**, 2334.
(177) Costa-Nunes, O.; Vohs, J. M.; Gorte, R. J. *J. Electrochem. Soc.* **2003**, *150*, A858.
(178) EG&G Technical Services, Inc. *Fuel Cell Handbook,* 5th ed.; DOE/NETL-2000; U.S. Department of Energy, Office of Fossil Energy, National Energy Technology Laboratory: Morgantown, WV, 2000, p 138.
(179) Kim, H.; Lu, C.; Worrell, W. L.; Vohs, J. M.; Gorte, R. J. *J. Electrochem. Soc.* **2002**, *149*, A247.
(180) Lee, S.-I.; Vohs, J. M.; Gorte, R. J. *J. Electrochem. Soc.*, submitted.
(181) Rodriguez, N. M.; Kim, M. S.; Baker, T. K. *J. Catal.* **1993**, *140*, 16.
(182) Sinfelt, J. H.; Carter, J. L.; Yates, D. J. C. *J. Catal.* **1972**, *24*, 283.
(183) Zhu, L.; Depristo, A. E. *J. Catal.* **1997**, *167*, 400.
(184) Kim, S.-K.; Kim, J.-S.; Han, J. Y.; Seo, J. M.; Lee, C. K.; Hong, S. C. *Surf. Sci.* **2000**, *453*, 47.
(185) Tao, T. T., U.S. Patent Application 20020015877, 2002.